

N 73-19386

NASA TECHNICAL  
REPORT



NASA TR R-399

NASA TR R-399

CASE FILE  
COPY

THE INFERENCE OF  
ATMOSPHERIC OZONE USING  
SATELLITE NADIR MEASUREMENTS  
IN THE  $1042 \text{ cm}^{-1}$  BAND

*by James M. Russell III and S. Roland Drayson*

*Langley Research Center*

*Hampton, Va. 23365*

1. Report No. NASA TR R-399	2. Government Accession No.	3. Recipient's Catalog No.	
4. Title and Subtitle THE INFERENCE OF ATMOSPHERIC OZONE USING SATELLITE NADIR MEASUREMENTS IN THE 1042 $\text{cm}^{-1}$ BAND		5. Report Date March 1973	6. Performing Organization Code
7. Author(s) James M. Russell III (Langley Research Center) and S. Roland Drayson (University of Michigan)		8. Performing Organization Report No. L-8635	10. Work Unit No. 160-44-64-02
9. Performing Organization Name and Address NASA Langley Research Center Hampton, Va. 23365		11. Contract or Grant No.	13. Type of Report and Period Covered Technical Report
12. Sponsoring Agency Name and Address National Aeronautics and Space Administration Washington, D.C. 20546		14. Sponsoring Agency Code	
15. Supplementary Notes The basic information presented herein was included in a thesis by the first author and was offered in partial fulfillment of the requirements for the degree of Doctor of Philosophy, University of Michigan, Ann Arbor, Michigan, July 1970.			
16. Abstract This report presents a description and detailed analysis of a technique for inferring atmospheric ozone information from satellite nadir measurements in the 1042 $\text{cm}^{-1}$ band. A method is formulated for computing the emission from the lower boundary under the satellite which circumvents the difficult analytical problems caused by the presence of atmospheric clouds and the water-vapor continuum absorption. The inversion equations are expanded in terms of the eigenvectors and eigenvalues of a least-squares-solution matrix, and an analysis is performed to determine the information content of the radiance measurements.  The results show that under favorable conditions there are only two pieces of independent information available from the measurements: the total ozone $u$ and the altitude $h_m$ of the primary maximum in the ozone profile. An error analysis shows that errors in $u$ are affected most by random radiance noise, lower boundary temperature errors, and ozone absorption-line intensity errors. Errors in $h_m$ are affected most by the former two errors and also by temperature-profile bias errors. The results when all errors are considered simultaneously indicate that it should ultimately be possible to determine $u$ to within 10 percent or less and to determine $h_m$ to within 1.5 km when the root-mean-square radiance noise level is 1 percent or less. The calculations are also made for various degrees of cloudiness in the troposphere. The data show that the presence of clouds does not seriously affect results as long as there is some contrast between the ozone spectrum and the lower boundary emission spectrum. Finally, the inversion technique is applied to radiances measured from a balloon over Palestine, Texas, and to Nimbus III satellite data measured over the Bahama Islands.			
17. Key Words (Suggested by Author(s)) Ozone Inversion Nadir measurements - information content Nimbus III satellite		18. Distribution Statement Unclassified - Unlimited	
19. Security Classif. (of this report) Unclassified	20. Security Classif. (of this page) Unclassified	21. No. of Pages 53	22. Price* \$3.00

THE INFERENCE OF ATMOSPHERIC OZONE USING SATELLITE  
NADIR MEASUREMENTS IN THE  $1042 \text{ cm}^{-1}$  BAND\*

By James M. Russell III  
Langley Research Center  
and S. Roland Drayson  
University of Michigan

SUMMARY

Only a small amount of information is contained in radiances measured vertically from a satellite in the  $1042 \text{ cm}^{-1}$  spectral region. Because of this low-information content, it is not necessary to use an elaborate function to characterize the vertical ozone distribution. A function was used that described the ozone profile in terms of just three parameters -  $p(\text{O}_3)_m$ ,  $p_m$ , and  $H$ . These correspond, respectively, to the maximum ozone partial pressure, the atmospheric pressure at the altitude of the maximum partial pressure, and a width factor. An inversion procedure was designed to select values for these parameters so that the computed ozone spectrum at the top of the atmosphere matched the measured spectrum in a least-squares sense. It was shown that the calculations should include the entire ozone band to obtain a maximum reduction of the effective random radiance noise. The atmosphere was divided into two broad layers: an upper layer containing pure ozone and a lower layer devoid of ozone containing the earth's surface and all the atmospheric water vapor and clouds. The problems connected with computing the water-vapor continuum and with considering clouds in the analysis were circumvented by following this procedure. The top of the lower layer was taken as the boundary under the satellite, and the effective temperature of the layer was used to compute the lower boundary emission in the equation of radiative transfer. The effective temperature could be found to be within 0.5 K or less by considering water-vapor line absorption in the calculations.

The least-squares solution for the three ozone parameters was expanded in terms of the eigenvectors and eigenvalues of a solution matrix. A subsequent analysis using synthetic clear-sky radiances showed that, under favorable conditions, measurements in the ozone band contain two pieces of independent information: the total ozone  $u$ , and the altitude  $h_m$  (or pressure  $p_m$ ), at the level of the maximum ozone partial pressure. An

---

\*The basic information presented herein was included in a thesis by the first author and was offered in partial fulfillment of the requirements for the degree of Doctor of Philosophy, University of Michigan, Ann Arbor, Michigan, July 1970.

error study revealed that errors in  $u$  are affected most by random radiance errors, lower boundary temperature errors, and ozone absorption-line intensity errors. Errors in  $h_m$  are affected most by the former two errors and by temperature-profile bias errors. When all error sources were considered simultaneously, the results showed that it should ultimately be possible to determine the total ozone to within 10 percent or less and to determine the altitude of the maximum partial pressure in the ozone profile to within 1.5 km when the root-mean-square radiance noise level is 1 percent or less. These latter calculations were repeated for varying degrees of cloudiness in the troposphere. The data showed that the presence of clouds did not seriously affect results as long as there was some contrast between the ozone spectrum and the effective lower boundary emission spectrum.

Next, the inversion technique was applied to balloon data measured over Palestine, Texas, and to the Nimbus III satellite data measured over Grand Turk Air Force Base in the Bahamas. The Palestine data contained very low radiance noise, and the corresponding inversion gave a value for  $u$  which was within about 3 percent of the value estimated from a nearby Dobson measurement. The value for  $h_m$  could not be accurately estimated, but the result obtained from the inversion was within the possible range of values indicated by past measurements made at the same general location and time of year. The Nimbus III data were very noisy by comparison to the balloon measurements, and this noise was reflected in the inversion. The inferred values for  $u$  and  $h_m$  were off by 76 percent and 6.3 km, respectively, when compared to values determined by a simultaneous ozonesonde observation. These errors are consistent with the predicted values of 96 percent and 7.7 km, respectively, as determined from the error-study results and the estimated random radiance noise in the Nimbus III data.

The application of the inversion technique to the Palestine and Nimbus data proved the validity of the inversion method and demonstrated the usefulness of the error study in predicting errors. The calculations also illustrated a critical need for further work to improve the accuracies of the absorption-line intensities. The basic difference between the Palestine and Nimbus data was the radiance noise level; the noise for the Palestine radiances was low, whereas the noise for the Nimbus data was comparatively high. It is believed that this is the underlying reason for the drastic differences in the inversion results for the two sets of data. If the absorption-line intensities had been known with greater precision, a much wider spectral interval could have been used in the calculations, thereby causing a significant reduction of the effective noise level in the Nimbus III data and a substantial improvement in the results. These results indicate that, unless absorption errors are decreased by empirical adjustments or other methods, calculations will have to be limited to a narrow spectral interval and, consequently, to low-noise data (less than 1 percent).

## INTRODUCTION

Ozone is only a minor atmospheric constituent; yet, it has held the attention of scientists ever since it was first suggested by the chemist Schönbein in 1840. The first conclusive evidence of an ozone layer in the atmosphere was deduced from ultraviolet absorption measurements made by Fabry and Buisson (ref. 1). Later, their conclusions were given theoretical support by the British geophysicist Chapman (ref. 2) who first explained the presence of ozone in the upper atmosphere by using photochemical principles. At about the same time, Dobson (ref. 3) published his paper describing the development of Fabry and Buisson's technique into a convenient method for routinely measuring the total ozone above an observer.<sup>1</sup>

After the work by Dobson and his coworkers the real meteorological significance of atmospheric ozone began to emerge. The systematic measurements of total ozone made possible by the Dobson instrument revealed a strong correlation between ozone amount and day-to-day weather variations. Later, with the advent of rocketsondes and high-altitude balloons, instruments were developed to measure, in situ, the vertical distribution of ozone as well as temperature and wind-field profiles. These measurements showed definite correlations between significant changes in the ozone partial pressure and changes in the temperature lapse rate and the wind-field frequency. (See, for example, ref. 4, or, for an extensive bibliography, ref. 5.) Other measurements showed an unquestionable dependence of total-ozone content on the position of the subtropical jet stream relative to the location of the ozone observations (refs. 6 and 7). Measurements by Godson (ref. 8) revealed correlations on a finer scale. He compared the 10-day running mean of 100-mb temperature with the total ozone for data taken over a 9-month period at Edmonton, Canada. His results showed that the average daily temperature variation was almost exactly correlated with the average daily variation in ozone amount.

As measurements of the vertical distribution of ozone accumulated and the photochemical theory was developed, important discrepancies were noticed between the distributions observed and the profiles predicted based on photochemistry. These discrepancies gave the first indication of the significant interrelationship between ozone content and atmospheric motions. Wulf (ref. 9) was apparently the first to propose a general circulation model which explained the ozone spring polar maximum. After his work, other papers were published concerning the relation between ozone and atmospheric motions, and the role of ozone in this regard became widely accepted. (See, for example, refs. 10 to 13.)

---

<sup>1</sup>This is the total (integrated) ozone amount in an atmospheric column of unit cross section which extends from the ground to the top of the atmosphere. The phrases "total ozone" and "ozone amount" will be used synonymously throughout this report.

The complex interplay between ozone and other atmospheric properties, especially atmospheric motions, caused widespread interest in global measurements of both total ozone and the vertical ozone distribution. In 1965, the National Academy of Sciences published a report outlining goals for an international observation program (ref. 14). The report cited several areas of research which would be advanced by global ozone measurements. These areas include the study of atmospheric dynamics in the region of the upper troposphere and lower stratosphere, the analysis and study of the circulation patterns of the Northern and Southern Hemispheres and the exchange processes that take place between them, the study of the mechanics of the tropospheric-stratospheric exchange process, the study of stratospheric photochemistry, and the study of atmospheric phenomena such as the "explosive warming" of the winter-spring stratosphere and the 26-month oscillation in the stratospheric wind and temperature.

The general interest in global-scale measurements of atmospheric ozone resulted in the conception of a number of satellite measurement techniques. These methods include the measurement of backscattered solar ultraviolet (UV) light (refs. 15 to 20), the measurement of visible and near UV solar radiation passing tangentially through the atmosphere (refs. 21 to 23), the measurement of the UV spectrum of a star during occultation from a satellite (ref. 24), and the use of laser transmission from the ground to a satellite or vice versa (ref. 5). The use of satellite nadir measurements in an infrared band ( $1042\text{ cm}^{-1}$ ) of ozone has also been suggested (ref. 25). This method is attractive since it does not contain many of the problems of the other techniques. In the infrared technique, the measurements are not restricted to specific geographic areas, and the method is applicable on both the day and night side of the planet. Also, since scattering is unimportant in the infrared spectral region, the analysis is comparatively simple and the multiple-scattering problem of the UV backscatter method does not exist.

Studies dealing with the determination of atmospheric ozone amounts from satellite nadir measurements in the infrared have been reported by Sekihara and Walshaw (ref. 26) and Prabhakara (ref. 27). A more recent paper by Prabhakara et al. (ref. 28) discusses inversion results for radiance measurements made with an Infrared Interferometer Spectrometer (IRIS) from on-board the Nimbus III satellite. In the latter report, the atmospheric ozone profile is represented by using empirical orthogonal functions. The atmospheric transmission due to ozone is computed by using a statistical band model, and the absorption-line parameters used in the computations are determined by trial and error with the help of an ozone sounding and Nimbus III radiance measurements. The water-vapor continuum is considered, but absorption by water-vapor line centers is not.

The present report presents the results of a detailed study of the nadir experiment. A different approach from that of Prabhakara et al. (ref. 28) is developed which reveals explicitly how many pieces of information are available from the measurements. The statistical band model is used to compute transmittances for an error study; but when the

inversion procedure is applied to balloon and satellite data, the line-by-line method is employed. No empirical corrections are imposed on the absorption-line parameters used in these calculations. A method is also presented to account for the presence of water-vapor line absorption in the ozone band.

### SYMBOLS

$B(\bar{\nu}, T)$	Planck radiance, watts/meter-steradian
$c$	velocity of light in a vacuum, centimeters/second
$\bar{d}$	mean spacing of absorption lines in an interval $\Delta\bar{\nu}$ wide, per centimeter
$E_0$	ground state energy per centimeter
$F_i$	ratio of perturbed to unperturbed line strength, dimensionless
$f(\bar{\nu}, \bar{\nu}_i)$	absorption-line profile function, centimeters
$g$	acceleration of gravity, centimeters/second <sup>2</sup>
$H$	width factor in Green's ozone profile function, dimensionless
$h_m$	altitude of maximum ozone partial pressure, kilometers
$K$	total number of atmospheric layers, dimensionless
$k$	Boltzmann constant, ergs/molecule-kelvin
$L$	Planck radiance for effective lower boundary temperature, watts/meter-steradian
$L(\bar{\nu}, \theta)$	spectral radiance, watts/meter-steradian
$\bar{l}$	effective length of a homogeneous absorption path, centimeters
$m$	mass per molecule, grams
$N$	total number of absorption lines in a band, dimensionless

$N'$	total number of absorption lines in an interval $\Delta\bar{\nu}$ wide, dimensionless
$n_s$	number density at standard temperature and pressure, per cubic centimeter
$P(S)$	probability distribution function for line intensity, dimensionless
$P(\bar{\nu})$	probability distribution function for line positions, dimensionless
$p$	atmospheric pressure, millibars
$p_m$	atmospheric pressure at level of maximum ozone partial pressure, millibars
$p(O_3)$	ozone partial pressure, micromillibars
$p(O_3)_m$	maximum ozone partial pressure in Green's ozone profile function, micromillibars
$q$	mass mixing ratio of an absorbing gas, dimensionless
$S_i$	intensity of $i$ th absorption line per atmosphere-centimeter <sup>2</sup>
$T$	atmospheric temperature, kelvins
$t$	variable of integration, dimensionless
$u$	integrated ozone mass in an atmospheric column of unit cross section, atmosphere-centimeter
$v_i$	$i$ th eigenvector, unit varies
$X$	a constant, dimensionless
$\alpha_{Di}$	Doppler half-width, per centimeter
$\alpha_{Li}$	Lorentz half-width, per centimeter
$\beta_{\bar{\nu}}$	mean absorption-line intensity for interval $\Delta\bar{\nu}$ per atmosphere-centimeter <sup>2</sup>
$\gamma_i$	unperturbed line strength in ground-state representation per atmosphere-centimeter <sup>2</sup>

$\epsilon_g(\bar{\nu})$	emissivity of lower boundary under a satellite, dimensionless
$\kappa(\bar{\nu}, p)$	absorption coefficient, per centimeter
$\lambda$	wavelength, centimeters
$\lambda_i$	ith eigenvalue, unit varies
$\bar{\nu}$	wave number, $1/\lambda$ , centimeter <sup>-1</sup>
$\sigma$	standard deviation of a random variable, unit varies
$\tau(\bar{\nu}, p)$	transmittance, dimensionless
$\phi(\bar{\nu})$	radiometer instrument function, dimensionless

## ANALYSIS

### Introduction

A spectrum of the upwelling thermal energy measured from a balloon above Palestine, Texas, on May 8, 1966, is shown in figure 1 (refs. 25 and 29). These data were obtained with a breadboard version of an IRIS in a test conducted by the High Altitude Engineering Laboratory of the University of Michigan for the Goddard Space Flight

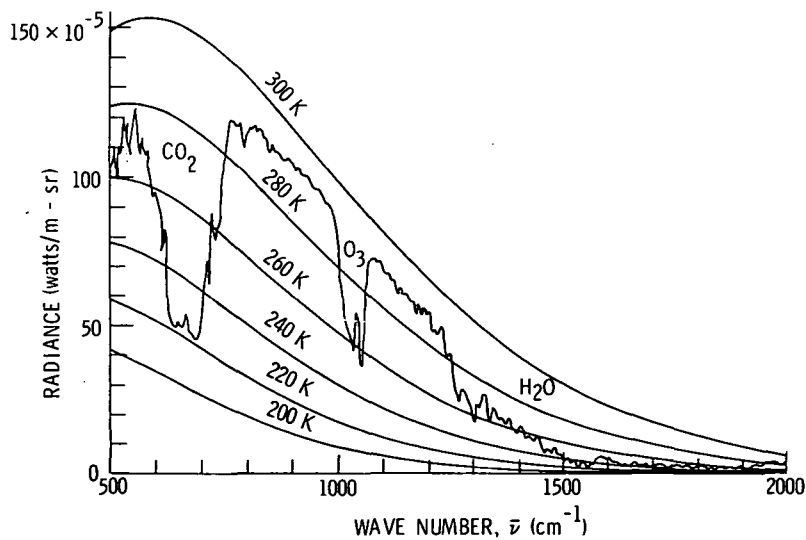


Figure 1.- Atmospheric emission spectrum acquired with a breadboard version of an IRIS instrument in a balloon flight at an altitude of 31.4 km on May 8, 1966, from Palestine, Texas (after Conrath, ref. 25). Smooth curves are plots of blackbody function at the indicated temperatures.

Center. The spectrum shows marked structure due to absorption by carbon dioxide, ozone, and water vapor. The magnitude of the energy at any given wave number in such a spectrum is a function of several variables. It depends on the temperature of the lower boundary (if the atmosphere is not opaque in the wave-number region of interest), on the temperature profile in the atmosphere, and on the amount and vertical distribution of gases that emit and absorb energy in the spectral pass band of the instrument. The upwelling energy also depends on the infrared reflectance properties of the lower boundary, but this dependence can usually be neglected. The fundamental relationship between the outgoing energy and properties of the earth-atmosphere system is the equation of radiative transfer (ref. 30). The form of the equation used in this paper is based on the following assumptions:

- (a) The atmosphere is plane-parallel.
- (b) Scattering at the wavelengths under consideration can be neglected.
- (c) Atmospheric refraction can be neglected.
- (d) The absorbing gases are in local thermodynamic equilibrium up to an altitude of 60 or 70 km (ref. 31).

If it is further assumed that the satellite instrument receives energy in a narrow cone in the vertical so that everywhere in the cone  $\sec \theta \approx 1$  (where  $\theta$  is the zenith angle), the equation of radiative transfer can be written in integral form as

$$\overline{L(\bar{\nu}_o, 0)} = \epsilon_g(\bar{\nu}_o) B[\bar{\nu}_o, T(p_g)] \overline{\tau(\bar{\nu}_o, p_g)} - \int_0^{p_g} B[\bar{\nu}_o, T(p)] \frac{d\overline{\tau(\bar{\nu}_o, p)}}{d(\log p)} d(\log p) \quad (1)$$

where  $\overline{L(\bar{\nu}_o, 0)}$  is the radiance at the top of the atmosphere for a given wave number  $\bar{\nu}_o$ ,  $T(p)$  is the atmospheric temperature,  $B[\bar{\nu}_o, T(p)]$  is the Planck radiance,  $\epsilon_g(\bar{\nu}_o)$  and  $p_g$  are the emissivity and pressure, respectively, at the lower boundary, and  $\overline{\tau(\bar{\nu}_o, p)}$  is the transmittance of the atmosphere from the satellite down to an arbitrary height where the atmospheric pressure is  $p$ . The bars above the symbols denote that these quantities are average values and the  $o$  subscript denotes the wave number at the center of the averaging interval. The averaging is performed according to some function which adequately represents the frequency response of the instrument.

The first term on the right in equation (1) represents the contribution to the radiance at the top of the atmosphere due to emission by the lower boundary (e.g., the earth's surface). The second term accounts for the contribution made by atmospheric emissions. Any descending energy which is reflected at the lower boundary has been neglected.

Atmospheric ozone information enters equation (1) through the transmittance  $\overline{\tau(\bar{\nu}_o, p)}$ .

Obviously, ozone data cannot be retrieved by using equation (1) unless the atmospheric temperature profile is known. It is assumed in this study that temperature data will be available from any one of the numerous satellite remote-sensing techniques which have been proposed (e.g., refs. 32 to 34). Before considering the problem of inverting equation (1) to obtain ozone information, there are two important topics which must be discussed: (1) the method used to compute the atmospheric transmittance, and (2) the method used to compute the lower boundary emission.

### Atmospheric Transmittances

The transmission of the atmosphere in the vicinity of  $1042 \text{ cm}^{-1}$  is influenced by water vapor and carbon dioxide as well as ozone. The water-vapor continuum absorption must be considered as well as absorption by water-vapor lines superimposed on the continuum. However, carbon-dioxide absorption is weak and it will be neglected in the current calculations. The estimated upper limit to the transmittance error caused by this assumption is about 5 percent based on calculations using the weak-line approximation. The actual error is probably only about 2 to 3 percent. Carbon-dioxide effects should not be neglected in future computations once the accuracies of the ozone transmittances are improved.

Water-vapor line absorption can be accurately computed if the vertical water-vapor distribution is known; and even if the vertical profile is not known, an adequate treatment is possible. However, the water-vapor continuum spectrum is difficult to model analytically since it arises from absorption in the wings of many lines located in distant-rotation and vibration-rotation bands. There are presently no totally acceptable theories available concerning this problem. Consequently, the influence of water vapor on the atmospheric transmittance in the ozone band will not be computed directly in this study. Instead, the effect will be treated as part of the problem of determining the lower boundary emission. The way this is done is discussed in the next subsection. Thus, the problem of computing the transmittance of the atmosphere is, in a sense, reduced to one of computing the transmittance due to ozone alone. Two methods of accomplishing this are described in the subsequent paragraphs.

The atmospheric transmittance at a wave number  $\bar{\nu}$  from the top of the atmosphere down to a height where the atmospheric pressure is  $p$  is given by

$$\tau(\bar{\nu}, p) = \exp - \left[ \int_0^p \kappa(\bar{\nu}, p) \frac{q(p)}{g(p)} dp \right] \quad (2)$$

where  $q(p)$  is the mass-mixing ratio of the absorbing gas,  $g(p)$  is the acceleration of gravity, and  $\kappa(\bar{\nu}, p)$  is the absorption coefficient. Assume now that the atmosphere is

divided into small incremental slabs in the vertical and consider the transmission through only one of these layers. If each layer is considered to be homogeneous, the transmittance for the  $j$ th layer is

$$\tau_j(\bar{\nu}, p_j) \approx \exp\left[-\kappa(\bar{\nu}, p_j)u_j\right] \quad (3)$$

where  $p_j$  is the mean pressure for the layer and  $u_j$  is the integrated mass across the layer given by

$$u_j = \int_{p_1}^{p_2} \frac{q(p)}{g(p)} dp \quad (4)$$

The pressures at the boundaries of the layer are given by  $p_1$  and  $p_2$ . Equation (3) is not an exact expression since, in reality, an atmospheric slab is inhomogeneous and the absorption coefficient varies with pressure across the layer. However, errors which arise in using equation (3) can be made as small as desired by using very thin slabs. Fundamentally, the problem of computing the transmittance of the atmosphere is one of calculating the absorption coefficient for each of the  $j$  layers in the atmosphere. This is not a simple problem since the absorption coefficient at any given wave number  $\bar{\nu}$  is the sum of the coefficients at  $\bar{\nu}$  due to each of a large number of absorption lines in a band, and each of these lines varies with pressure and temperature.

Consider first the absorption coefficient at  $\bar{\nu}$  due to a single line centered at a wave number  $\bar{\nu}_i$  in the band. For this  $i$ th line and the  $j$ th atmospheric layer,

$$\kappa_i(\bar{\nu}, p_j) = S_i f(\bar{\nu}, \bar{\nu}_i) \quad (5)$$

where  $S_i$  is the line intensity or strength and  $f(\bar{\nu}, \bar{\nu}_i)$  is the profile function which describes the line shape. The profile function is normalized so that

$$\int_0^{\infty} f(\bar{\nu}, \bar{\nu}_i) d\bar{\nu} = 1 \quad (6)$$

and

$$S_i = \int_0^{\infty} \kappa_i(\bar{\nu}, p_j) d\bar{\nu} \quad (7)$$

The absorption coefficient varies with altitude because of changes in both the line strength and the profile function. The line strength contributes to the variation through a

temperature dependence. The relationship used by Clough and Kneizys (ref. 35) for ozone is given by

$$S_i(T_j) = X\gamma_i F_i \left(\frac{273}{T_j}\right)^{5/2} \exp\left[-\frac{E_o}{kT_j}\right] \quad (8)$$

where  $X$  is a constant,  $\gamma_i$  is the unperturbed line strength in the ground-state representation,  $F_i$  is the ratio of perturbed to unperturbed line strength,  $E_o$  is the ground-state energy, and  $k$  is the Boltzmann constant. The profile function varies with altitude because of both a temperature and a pressure dependence. The variation in the profile function for the range of physical conditions considered here can be described by two limiting cases: the Lorentz and Doppler line shapes. A third case, the natural-line shape, can be neglected since the width of the natural broadened line is much smaller than the width for either of the other two cases.

The Lorentz line shape is caused by molecular collisions and is described by the function

$$f_L(\bar{\nu}, \bar{\nu}_i) = \frac{1}{\pi} \left[ \frac{\alpha_{Li}}{(\bar{\nu} - \bar{\nu}_i)^2 + \alpha_{Li}^2} \right] \quad (9)$$

where  $\alpha_{Li}$  is the Lorentz half-width at half-maximum. The half-width depends on pressure and temperature according to

$$\alpha_{Li}(T_j, p_j) = \alpha_{oi} \frac{p_j}{p_o} \sqrt{\frac{T_o}{T_j}} \quad (10)$$

where  $\alpha_{oi}$  is the half-width at temperature  $T_o$  and pressure  $p_o$ .

The Doppler line shape arises because of thermal motions of the molecules. In this case,

$$f_D(\bar{\nu}, \bar{\nu}_i) = \left(\frac{\ln 2}{\pi \alpha_{Di}^2}\right)^{1/2} \exp(-x^2) \quad (11)$$

where

$$x = \left(\frac{\ln 2}{\alpha_{Di}^2}\right)^{1/2} (\bar{\nu} - \bar{\nu}_i)$$

and where  $\alpha_{Di}$  is the Doppler half-width at half-maximum which is expressed by

$$\alpha_{Di} = \frac{\bar{\nu}_i}{c} \left( \ln 2 \frac{2kT_j}{m} \right)^{1/2} \quad (12)$$

The quantity  $m$  is the mass per molecule in grams.

The transition from the region of the atmosphere where one limiting shape is important to the region where the other dominates is not abrupt. Therefore, a range of pressures is encountered where both thermal and collisional effects are important in determining the absorption-line profile. Under these conditions, the correct line shape is given by a convolution of the Doppler and Lorentz shapes. This shape, called the Voigt function, is represented by

$$f_V(\bar{\nu}, \bar{\nu}_i) = \left( \frac{\ln 2}{\pi^3 \alpha_{Di}^2} \right)^{1/2} y \int_{-\infty}^{\infty} \frac{e^{-t^2}}{y^2 + (x - t)^2} dt \quad (13)$$

where

$$y = \frac{\alpha_{Li}}{\alpha_{Di}} (\ln 2)^{1/2}$$

So far, the main concern has been with a single absorbing line and it has been shown how the absorption coefficient for this line varies as a function of the atmospheric parameters, pressure, and temperature. To compute the integrated effect of all lines in a band on the absorption at a given wave number  $\bar{\nu}$ , it is necessary to sum the values of absorption coefficients at  $\bar{\nu}$  due to each absorption line. Thus, for  $N$  lines, the monochromatic absorption coefficient is

$$\kappa(\bar{\nu}, p_j) = \sum_{i=1}^N \kappa_i(\bar{\nu}, p_j) \quad (14)$$

The monochromatic transmittance is computed by inserting equation (14) into equation (2); and then the average value is calculated according to the following equation:

$$\overline{\tau(\bar{\nu}, p)} = \frac{\int_{\bar{\nu}_1}^{\bar{\nu}_2} \tau(\bar{\nu}, p) \phi(\bar{\nu}) d\bar{\nu}}{\int_{\bar{\nu}_1}^{\bar{\nu}_2} \phi(\bar{\nu}) d\bar{\nu}} \quad (15)$$

where  $\bar{\nu}_1$  and  $\bar{\nu}_2$  are the bounds of the spectral interval spanned by the instrument function  $\phi(\bar{\nu})$ . Equation (14) is a lengthy calculation because of the large number of lines normally found in an absorption band. The equation is also complicated because of the requirement that the computations be done for all  $j$  layers in the atmosphere, in which case the line strength and shape variability must be included. These difficulties prompted the development of the band-model concept to compute transmittances. In this approach, the actual distributions of absorption-line positions and intensities are simulated; and, instead of computing equation (14) and the average transmittance from equation (15) directly, the calculations are approximated by an analytical integration using the assumed distributions of the line parameters. Even though band models are still frequently used today, it is now possible, because of the existence of high-speed computers, to perform the calculations directly by the direct-integration (or line-by-line) method (refs. 36 and 37). The advantages and disadvantages of each of these approaches were discussed by Drayson (ref. 38) and will not be repeated here. Both procedures were used in this present work and a brief description of each method follows.

The direct-integration method is numerically the most accurate of the two techniques. The method predicts the absorption almost exactly if the absorption-line parameters are known precisely. In the program developed by Drayson and Young (ref. 37) the monochromatic transmittance is computed at various wave numbers in the absorption band. Since the values are computed monochromatically, the transmittance from the top of the atmosphere down to a height where the pressure is  $p$  can be computed by multiplying the transmittances for each of  $K$  atmospheric layers. Accordingly,

$$\tau(\bar{\nu}, p) = \prod_{j=1}^K \tau_j(\bar{\nu}, p_j) \quad (16)$$

where the symbol  $\Pi$  denotes multiplication. These monochromatic transmittances are then averaged over  $0.1 \text{ cm}^{-1}$  intervals at the bottom of each  $K$ th layer. With this technique, the atmosphere can be divided into a series of thin homogeneous layers, each of which has values of pressure and temperature equal to the average values for the layer. Since each transmittance value is computed for a thin atmospheric layer, it is relatively easy to include the appropriate absorption-line shape and intensity for that region of the atmosphere in the calculations. The Drayson and Young program includes all three absorption-line broadening regimes, it allows for the variation of line half-width with wave number, and it accounts for the variation of line intensity with temperature. The chief drawback to using the method is that it is very time consuming, even when modern, high-speed computers are used. Consequently, the technique was used here only when a high degree of computational accuracy was desired, such as in calculating the effect of line-

strength temperature dependence on transmittance and in applying the inversion method developed in this paper to the Nimbus III and Palestine, Texas, flight data. The error-study transmittances were calculated by using the random exponential band model (refs. 39 and 40). A description of this model follows.

The major gain in using the band-model technique rather than the line-by-line method is a great reduction in the time required for a calculation. The line-parameter distribution functions used with the most success in the ozone band are a random distribution of line positions and an exponential distribution of line intensities. (See, for example, ref. 41.) The probability distribution function for the line positions is  $P(\bar{\nu}) = \frac{1}{\Delta\bar{\nu}}$  where  $\Delta\bar{\nu}$  is the width of the spectral interval, and the function for line intensities is

$$P(S) = \frac{1}{\beta_{\bar{\nu}}} \exp\left(-\frac{S}{\beta_{\bar{\nu}}}\right) \quad (17)$$

where  $\beta_{\bar{\nu}}$  is the mean absorption-line intensity for the interval  $\Delta\bar{\nu}$ . With these distributions, the average transmittance at a wave number  $\bar{\nu}$  through a single atmospheric layer is (ref. 42) given as

$$\overline{\tau(\bar{\nu}, p_j)} = \exp(-\omega) \quad (18)$$

The argument of the exponential is computed as follows:

$$\omega = \frac{1}{\bar{d}} \int_{-\infty}^{\infty} \frac{\beta_{\bar{\nu}} f(\bar{\nu}, \bar{\nu}_i) u_j}{1 + \beta_{\bar{\nu}} f(\bar{\nu}, \bar{\nu}_i) u_j} d\bar{\nu} \quad (19)$$

where  $\bar{d} = \frac{\Delta\bar{\nu}}{N'}$  is the mean line spacing and  $N'$  is the number of lines in the interval  $\Delta\bar{\nu}$ . Since the transmittance computed with the band model is an average value for the spectral interval, the transmittance through  $K$  layers cannot be computed simply by multiplying the values for each  $j$ th layer (ref. 42, p. 123). Instead, the transmittance must be calculated for an equivalent homogeneous slab defined by the  $K$  layers. The reduction of an arbitrary path in the atmosphere to an equivalent homogeneous path is usually done by means of the Curtis-Godson approximation (e.g., ref. 43). This approximation is not very accurate for atmospheric ozone (refs. 44 and 45), but the accuracy is good enough that the method can still be used in the error-study calculations discussed later. There are two other approximations which will be used in the band-model calculations. It is assumed that purely collisional line broadening is valid throughout the range of altitudes considered and that the line intensities do not vary with temperature. The

assumption of collisional broadening causes a small transmittance error above an altitude of approximately 30 km since in this region the Voigt profile function is important (ref. 31). However, the estimated maximum error is only about 2 percent according to the correction table published by Gille and Ellingson (ref. 46). The effect of neglecting the line-intensity temperature dependence is discussed in a subsequent section. These approximations cannot be used in precision calculations but they should have little effect upon the error-study results. Goody (ref. 42) integrated equation (19) for a Lorentz profile function to give

$$\overline{\tau(\bar{\nu}, p_k)} = \exp \left[ - \frac{(\beta_{\bar{\nu}}/\bar{d})\bar{u}_k}{\left\{ 1 + 2 \left[ \frac{\beta_{\bar{\nu}}}{2\pi\alpha_{Lo}(\bar{\nu})} \right] \bar{l}_k \right\}^{1/2}} \right] \quad (20)$$

where  $\bar{l}_k$  and  $\bar{u}_k$  are the effective length and absorber amount, respectively, of the homogeneous path and  $\alpha_{Lo}(\bar{\nu})$  is the Lorentz half-width at the wave number  $\bar{\nu}$  and at standard temperature and pressure. The subscript  $k$  refers to the effective value for a homogeneous slab defined by  $K$  layers. The methods for computing the various quantities in equation (20) are discussed in appendix A. A spectral interval of  $5 \text{ cm}^{-1}$  was used in all calculations with equation (20) to simulate the resolution of an IRIS.

All transmittance calculations were based on ozone absorption-line strength and position data published by Clough and Kneizys (refs. 35 and 47). A good indication of errors that may exist in these data can be obtained by comparing theoretical and experimental absorption spectra for a homogeneous path. S. R. Drayson and C. Young of the University of Michigan have done this by using their line-by-line technique and experimental measurements made by McCaa and Shaw (ref. 48). The experimental values are believed to be accurate to within 10 percent or less. A comparison of the computed and experimental spectra for a set of conditions similar to those encountered in the atmosphere is shown in figure 2. The theory predicts too little absorption on the low wave-number side of the band and too much absorption on the high wave-number side. Also, the discrepancies are much greater than the experimental inaccuracies. It appears, therefore, that there are large errors in the absorption-line parameters. Nevertheless, no attempt is made in this study to correct the values of these parameters either empirically or by other means. Empirical adjustments can be a useful means of correcting the absorption parameters as shown by Prabhakara et al. (ref. 28). However, corrections made for atmospheric conditions prevailing above one region of the globe may not necessarily be appropriate corrections for a different region. Ultimately, therefore, it appears that the most satisfactory approach is to use absorption parameters based only

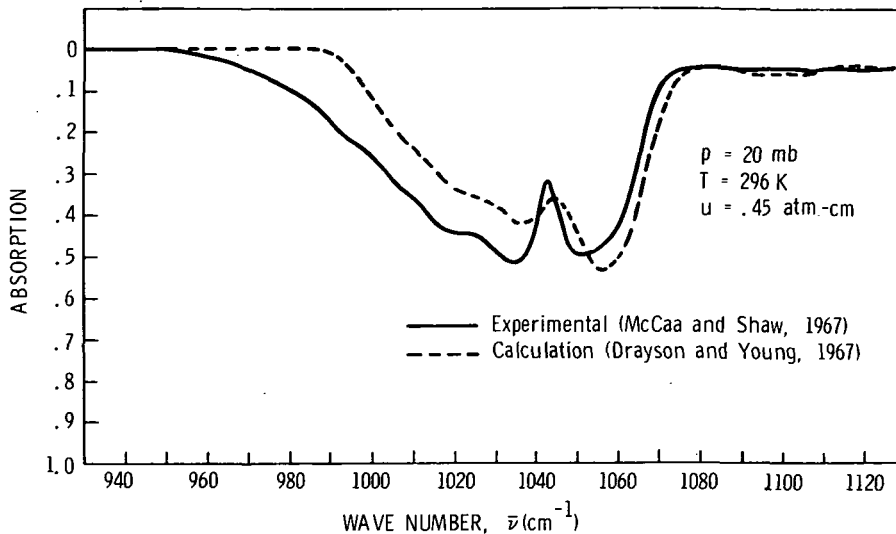


Figure 2.- Comparison of experimental and calculated absorption in the  $1042 \text{ cm}^{-1}$  ozone band.

on a knowledge of the physics of the ozone molecule as is done in this report. The effects of absorption-parameter errors on results are discussed in the error-study section of this paper.

#### Lower Boundary Emission

Background emission from the underlying boundary can significantly alter the ozone spectrum measured at the top of the atmosphere. Sometimes, in high-latitude areas of the globe, the combined effect due to atmospheric and lower boundary emissions can create the condition where there is little or no contrast between the background emission spectrum and the ozone spectrum. Under these conditions, it may be difficult or impossible to determine ozone information from satellite measurements. These effects are discussed in appendix B. The following subsection describes the technique used in this study to compute the lower boundary emission.

The lower boundary emission is clearly represented by the first term on the right-hand side of equation (1). However, the evaluation of this term is not straightforward. For example, if the underlying boundary is the earth's surface, it is difficult to determine the surface conditions which should be used. The field of view of a satellite instrument covers a large area; and since both the surface temperature and surface emissivity vary with terrain, appropriate average values must be found for these quantities. If the sky contains clouds, the emissivity of the clouds must be considered and the emissions from the clouds and surface must be weighted in some way according to the percentage of cloud cover. The problem is further compounded by the presence of the water-vapor continuum absorption which is difficult to compute. This absorption attenuates the energy emitted

by the earth's surface before it reaches the top of the atmosphere. But these difficulties can be circumvented to a large extent by using the fact that the ozone partial pressure is small in the troposphere. This property of atmospheric ozone makes it possible to divide the atmosphere into two broad layers: an upper layer containing pure ozone and a lower layer devoid of ozone containing the earth's surface and all the atmospheric water vapor and clouds. This approach greatly simplifies the problem as will be seen in the subsequent paragraphs.

If the spectral interval is sufficiently wide so that there is no correlation between  $O_3$  and  $H_2O$  absorption, then the transmission through a water-vapor ozone atmosphere is given by (ref. 42, p. 123)

$$\overline{\tau(\bar{\nu}, p)} = \overline{\tau(H_2O, \bar{\nu}, p)} \quad \overline{\tau(O_3, \bar{\nu}, p)} \quad (21)$$

If, for clarity, the arguments of the variables in equation (1) are dropped and the subscript  $g$  is used to denote the lower boundary and  $o$  to denote the top of the atmosphere, the equation can be written

$$\bar{L}_o = \epsilon_g B_g \bar{\tau}_g(H_2O) \tau_g(O_3) + \int_{\tau_g}^1 B d[\bar{\tau}(H_2O) \bar{\tau}(O_3)] \quad (22)$$

where the relation of equation (21) is used. Expanding equation (22) gives

$$\bar{L}_o = \epsilon_g B_g \bar{\tau}_g(H_2O) \bar{\tau}_g(O_3) + \int_{\tau_g(H_2O)}^1 B \bar{\tau}(O_3) d\bar{\tau}(H_2O) + \int_{\tau_g(O_3)}^1 B \bar{\tau}(H_2O) d\bar{\tau}(O_3) \quad (23)$$

Consider now figure 3 which shows typical water vapor, ozone, and temperature distributions and which illustrates the two-layer concept. Since the water-vapor content is very small in the stratosphere and the  $O_3$  content is small in the troposphere,  $\bar{\tau}(O_3) \approx \text{Constant}$  in the lower layer and  $\bar{\tau}(H_2O) \approx 1$  (in the spectral vicinity of  $1042 \text{ cm}^{-1}$ ) in the upper region. For these conditions  $\bar{\tau}_g(O_3) \approx \bar{\tau}_r(O_3)$  where  $\bar{\tau}_r(O_3)$  is the transmittance from the top of the atmosphere down to the bottom of the ozone layer. Therefore, equation (22) can be written

$$\bar{L}_o = \left[ \epsilon_g B_g \bar{\tau}_g(H_2O) + \int_{\tau_g(H_2O)}^1 B d\bar{\tau}(H_2O) \right] \bar{\tau}_r(O_3) + \int_{\tau_r(O_3)}^1 B d\bar{\tau}(O_3) \quad (24)$$

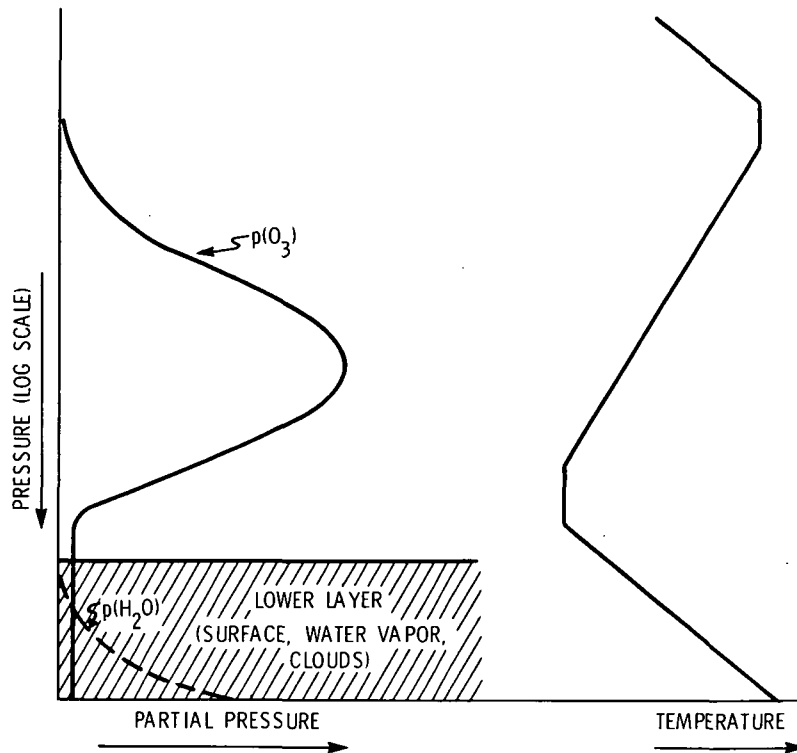


Figure 3.- The two-layer concept.

where the bracketed portion of the first term on the right-hand side is the emission from the lower layer. If the water-vapor line-absorption spectrum is excluded for the present and the emissivity ( $\epsilon_g$ ) is considered to be constant in the spectral regions immediately adjacent to and including the ozone band, the spectrum at the top of the atmosphere can be viewed as consisting of the Planck radiance of the lower layer at some effective temperature  $T_{eff}$  and the superimposed absorption spectrum of a pure ozone layer. The temperature  $T_{eff}$  will depend on the surface, water vapor, and cloud conditions. The value of  $T_{eff}$  is determined by selecting a value which gives a match between the Planck radiance and the measured spectrum on either side of the ozone band.

Since the measurements contain noise,  $T_{eff}$  is found by using the method of least squares fitting a Planck function through the maximum radiance points of the measured spectrum. This is illustrated by the dashed line in the bottom spectrum of figure 4. The spectral structure in figure 4 is due to ozone absorption and line absorption by water vapor. It is not obvious that water-vapor line structure exists in the part of the spectrum where ozone absorbs. This is because the effects of the lines are reduced in the center of the band by absorption of the upwelling lower boundary energy in the ozone layer, and they are hidden in other spectral regions because of the slope of the ozone spectrum. Nevertheless, line structure is present throughout the band as part of the background emission. This is illustrated in the lower spectrum of figure 4 by the dotted water-vapor

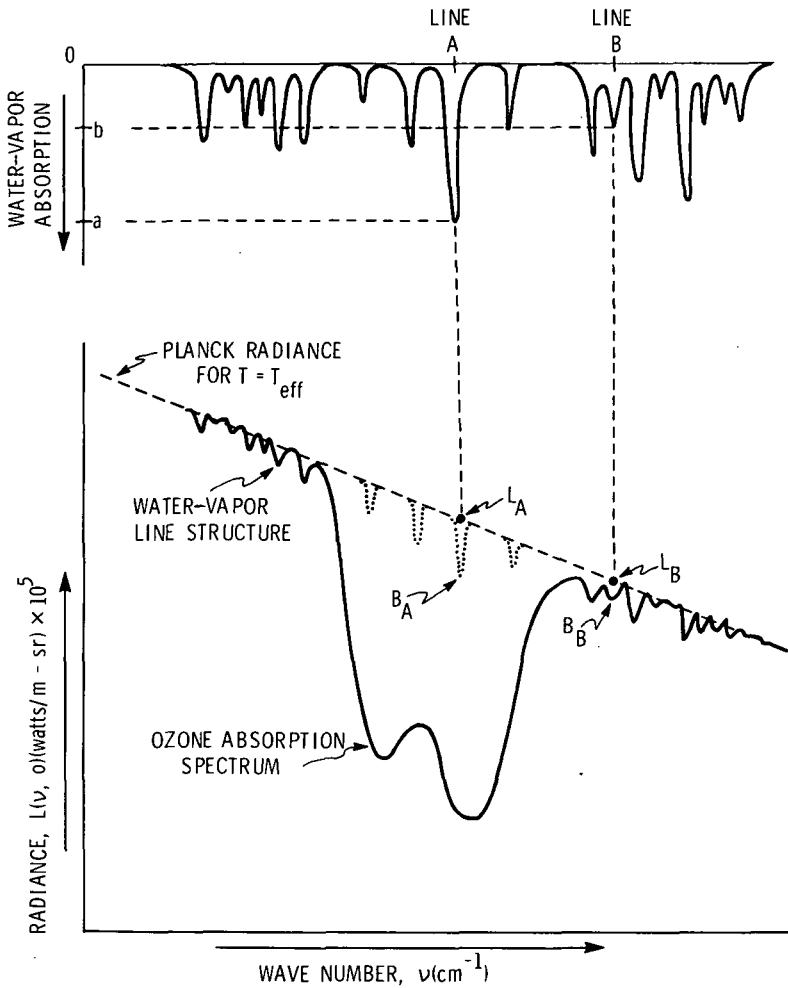


Figure 4.- Sketch of typical ozone and water-vapor absorption spectra.

lines. (The magnitudes of these lines are not drawn to scale relative to the ozone spectrum, and the positions do not necessarily coincide with the positions in an actual water-vapor spectrum.) The effect of water-vapor lines is considered by computing a line-absorption spectrum for tropospheric water vapor by using the direct-integration technique. The top spectrum in figure 4 illustrates this computation. Preferably, the calculations would be done by using an actual sounding of the water-vapor altitude distribution. However, if there is no sounding available, the mean climatological profile can be used. After computing the water-vapor line spectrum, the water-vapor absorption at any point in the measured spectrum can be predicted based on the relative absorption in the computed water-vapor line spectrum. For example, suppose it is desired to compute the background emission  $B_A$  at the position of the line A in the measured spectrum. The ratio of the absorption by line A to that by line B in the computed line spectrum is  $a/b$ . Therefore, the lower boundary emission  $B_A$  at the position of water-vapor line A is

$$B_A = L_A - \left(\frac{a}{b}\right) (L_B - B_B) \quad (25)$$

where  $L_A$  and  $L_B$  are the Planck radiances at the positions of lines A and B for  $T = T_{\text{eff}}$ , and  $B_B$  is the measured upwelling radiance at the position of line B. This method was used with the Nimbus and Palestine, Texas, flight data. The direct-integration method and the  $\text{H}_2\text{O}$  line parameters of Benedict and Calfee (ref. 49) were used to compute the line absorption. Some calculations were done for water-vapor absorption centers located outside the spectral region of ozone absorption. It was possible with this procedure to evaluate the accuracy of lower boundary emission values determined by this method. The calculations showed that the background emission could be computed to within  $5 \times 10^{-5}$  watt/m-sr or less. This corresponds to an effective background-temperature error of  $\leq 0.5$  K in the wings of the ozone band and a smaller error toward the center. The background emission computed in this manner at various wave numbers can be used to replace quantity  $\epsilon_g(\bar{\nu}_0) B[\bar{\nu}_0, T(p_g)]$  in the first term on the right-hand side of equation (1). When this is done, the transmittances in that equation correspond to the transmittances of the atmosphere due to ozone alone.

#### The Inversion Method

The problem to be solved is the following: given the temperature variation with altitude, find an atmospheric ozone profile which gives a match between the radiance  $\bar{L}_c(\bar{\nu}_0, 0)$  which is calculated with equation (1) and the radiance  $\bar{L}_m(\bar{\nu}_0, 0)$  which is measured. Equation (1) behaves like a Fredholm integral equation of the first kind (ref. 32). Therefore, an infinite number of ozone profiles can be found which will provide a radiance match to within any given error limits. This family of results will include a multitude of solutions which bear no physical resemblance to a realistic ozone profile. Therefore, one is faced with the problem of filtering out those solutions which are mathematically valid but which are physically unrealistic. This is normally accomplished by preselecting a form of the solution which is known to be physically valid based on other information, that is, climatology. (For example, in the temperature-inversion problem discussed by Wark and Fleming (ref. 32), the temperature solution is expressed in terms of empirical orthogonal functions which are determined from a large number of temperature soundings in a given area of the globe.) (See ref. 50.)

A function is needed which adequately represents the general shape of the vertical ozone distribution described in any one of a number of references (e.g., refs. 51 to 54). It would be desirable to include enough parameters in the function to define the dominant features, that is, the magnitudes and altitudes (or pressure levels) of the three major peaks in the profile. However, because of the low-information content of the measurements (ref. 55), the most that can be expected from an inversion is data that define the

gross features of atmospheric ozone, that is, properties such as the total ozone, the altitude where the main peak in the profile occurs, and the value of the maximum partial pressure at the main peak. A function which characterizes the profile by just a few parameters is all that is required, since greater detail is not available from the measurements. Green (ref. 56) used a relationship that is well suited for this purpose. It is expressed in terms of the value of the maximum partial pressure  $p(\text{O}_3)_m$ , the atmospheric pressure  $p_m$  at the altitude where the maximum partial pressure occurs, and a width factor  $H$ . The function is given by the following equation:

$$p(\text{O}_3) = 4 p(\text{O}_3)_m \frac{e^x}{(1 + e^x)^2} \quad (26)$$

where

$$x = \frac{\log(p/p_m)}{H}$$

and where  $p(\text{O}_3)$  is the ozone partial pressure. The function is used in this study to describe the ozone profile in a range of altitudes starting near the tropopause and extending upward. The partial pressure in the troposphere is considered to be constant. A plot of this function is shown in a subsequent figure.

The goal of the inversion method is to select values for the three parameters  $p(\text{O}_3)_m$ ,  $p_m$ , and  $H$  which give a match between  $\bar{L}_c(\bar{\nu}_o, 0)$  and  $\bar{L}_m(\bar{\nu}_o, 0)$  according to a criterion which is discussed subsequently. The initial step in the solution procedure is to make a linear approximation for the relationship between  $\bar{L}_m(\bar{\nu}_o, 0)$ ,  $\bar{L}_c(\bar{\nu}_o, 0)$ , and the three parameters as follows:

$$\bar{L}_m(\bar{\nu}_o, 0) = \bar{L}_c(\bar{\nu}_o, 0) + \frac{\partial \bar{L}_c(\bar{\nu}, 0)}{\partial p(\text{O}_3)_m} \Delta p(\text{O}_3)_m + \frac{\partial \bar{L}_c(\bar{\nu}, 0)}{\partial p_m} \Delta p_m + \frac{\partial \bar{L}_c(\bar{\nu}, 0)}{\partial H} \Delta H \quad (27)$$

This is a Taylor's series expansion with the higher order terms truncated. To determine three parameters, at least three equations must be used. The required three equations can be written from equation (27) to correspond to measured radiances at three wave numbers. Dropping the parentheses and using a numerical subscript to denote the first, second, and third wave-number centers gives

$$\left. \begin{aligned}
\bar{L}_{m1} &= \bar{L}_{c1} + \frac{\partial \bar{L}_{c1}}{\partial p(\text{O}_3)_m} \Delta p(\text{O}_3)_m + \frac{\partial \bar{L}_{c1}}{\partial p_m} \Delta p_m + \frac{\partial \bar{L}_{c1}}{\partial H} \Delta H \\
\bar{L}_{m2} &= \bar{L}_{c2} + \frac{\partial \bar{L}_{c2}}{\partial p(\text{O}_3)_m} \Delta p(\text{O}_3)_m + \frac{\partial \bar{L}_{c2}}{\partial p_m} \Delta p_m + \frac{\partial \bar{L}_{c2}}{\partial H} \Delta H \\
\bar{L}_{m3} &= \bar{L}_{c3} + \frac{\partial \bar{L}_{c3}}{\partial p(\text{O}_3)_m} \Delta p(\text{O}_3)_m + \frac{\partial \bar{L}_{c3}}{\partial p_m} \Delta p_m + \frac{\partial \bar{L}_{c3}}{\partial H} \Delta H
\end{aligned} \right\} \quad (28)$$

An iterative procedure is used to determine the final values of the three parameters  $p(\text{O}_3)_m$ ,  $p_m$ , and  $H$ . After making initial guesses for the parameters, the quantities  $\bar{L}_{ci}$  are computed by using equations (26), (3) or (20), and (1). The partial derivatives are computed in a similar manner by letting one parameter at a time change by a small amount in order to obtain the differentials. Upon solving for  $\Delta p(\text{O}_3)_m$ ,  $\Delta p_m$ , and  $\Delta H$ , these quantities are added to the initial guesses and the process is repeated until some convergence criteria are met.

The system of equations (28) could be solved directly without further manipulations. However, since the measured radiances will contain noise, it is desirable to use a least-squares fitting procedure. It is also desirable to use an overdetermined solution method; that is, use many more equations than are needed to determine the three parameters. By using a large number of measurements (preferably measurements covering the entire ozone band) and by using a least-squares solution, the standard deviation of the radiance noise can, in effect, be reduced.<sup>2</sup> So, if  $M$  measurements are used, instead of having just three equations, the system of equations (28) will have  $M$  equations. This system of  $M$  equations can be expressed in matrix form as follows:

$$\Delta L = Q R \quad (29)$$

where  $\Delta L$  is an  $M \times 1$  matrix defined by the differences  $(\bar{L}_{mi} - \bar{L}_{ci})$ ,  $Q$  is the  $M \times 3$  matrix of partial derivatives, and  $R$  is the  $3 \times 1$  matrix defined by the perturbation terms. The least-squares solution to equation (29) is easily shown to be

---

<sup>2</sup> Currently, it is not possible to use the entire band because of the magnitudes and differences in sign of absorption errors in various parts of the band. (Refer to fig. 2.) This emphasizes the importance of further work to improve the accuracies of the absorption-line parameters.

$$R = (Q^T Q)^{-1} (Q^T \Delta L) \quad (30)$$

where the superscripts T and -1 denote the matrix transpose and inverse, respectively.

Equation (30) is unstable in its present form when a small error is added to  $\Delta L$ ; that is, a small error in  $\Delta L$  will cause a vastly different solution than when the error is zero. This is because the matrix  $(Q^T Q)^{-1}$  is almost singular. This condition arises because of the high degree of overlap of the weighting functions. Stating this another way, the solution is unstable because it depends on information which is not available from the measurements. When this solution occurred in the temperature-inversion problem, the procedure was to introduce a smoothing matrix and a smoothing parameter  $\gamma w$  (ref. 32). The value of  $\gamma w$ , which depends upon the errors that are present, was determined by a trial-and-error procedure. The approach preferred here is to express the solution in terms of eigenvectors and eigenvalues. This approach has been used by Drayson (ref. 57) and also by Mateer (ref. 58) to deal with the instability of equation (30). The advantage of this procedure is that it will show explicitly how many pieces of independent information are available from the measurements.

The matrix  $(Q^T Q)$  is real, symmetric, and positive definite. Therefore, its eigenvalues will be real and positive. Suppose that the eigenvalues of  $(Q^T Q)$  designated  $\lambda_1$ ,  $\lambda_2$ , and  $\lambda_3$  are ordered so that  $\lambda_1 \geq \lambda_2 \geq \lambda_3$  with corresponding orthonormal eigenvectors  $v_1$ ,  $v_2$ , and  $v_3$ . The column matrix  $(Q^T \Delta L)$  can be expressed in terms of the eigenvectors of  $(Q^T Q)$  by

$$(Q^T \Delta L) = \sum_{i=1}^3 b_i v_i \quad (31)$$

where  $b_i$  is a constant for each eigenvector. Now, equation (30) becomes

$$R = (Q^T Q)^{-1} \sum_{i=1}^3 b_i v_i = \sum_{i=1}^3 b_i (Q^T Q)^{-1} v_i \quad (32)$$

It is known by a property of eigenvalues and eigenvectors that

$$(Q^T Q)^{-1} v_i = \frac{1}{\lambda_i} v_i \quad (33)$$

Therefore,

$$R = \sum_{i=1}^3 \frac{b_i}{\lambda_i} v_i \quad (34)$$

Expanding equation (34) gives

$$\begin{pmatrix} \Delta p(O_3)_m \\ \Delta p_m \\ \Delta H \end{pmatrix} = \begin{pmatrix} b_1 \frac{a_{11}}{\lambda_1} + b_2 \frac{a_{12}}{\lambda_2} + b_3 \frac{a_{13}}{\lambda_3} \\ b_1 \frac{a_{21}}{\lambda_1} + b_2 \frac{a_{22}}{\lambda_2} + b_3 \frac{a_{23}}{\lambda_3} \\ b_1 \frac{a_{31}}{\lambda_1} + b_2 \frac{a_{32}}{\lambda_2} + b_3 \frac{a_{33}}{\lambda_3} \end{pmatrix} \quad (35)$$

where  $a_{ji}$  gives the components of the eigenvectors  $v_i$ . That is,

$$v_i = \begin{pmatrix} a_{1i} \\ a_{2i} \\ a_{3i} \end{pmatrix} \quad (36)$$

The errors in the system can be viewed as being contained in the constants  $b_i$  since, in order to determine the values of  $b_i$ , the matrix  $(Q^T \Delta L)$  is used. The errors arise in  $Q$  and in  $\Delta L$  which, as previously stated, is the difference  $(L_{mi} - L_{ci})$ , where  $i$  is the wave-number subscript. Errors in measurement appear through  $\bar{L}_{mi}$  and all other errors occur in computing  $\bar{L}_{ci}$ . In reality, therefore, equation (34) can be written

$$R = \sum_{i=1}^3 \frac{b_{oi}}{\lambda_i} v_i + \sum_{i=1}^3 \frac{e_i}{\lambda_i} v_i \quad (37)$$

where  $b_{oi}$  is the value of the constant with no error and  $e_i$  represents the error contribution. The reason for the instability of equation (30) now becomes clear. If  $\lambda_i$  is very small, then the error term will be very important and could dominate the solution. When recalling that the values of  $\lambda_i$  are ordered, when equation (37) is expanded, it may be assumed that the second and/or third eigenvalues will be so small and the resulting

error terms will be so large that the iteration procedure will either be unstable or will converge to a physically unrealistic solution. It can be shown (ref. 57) that the eigenvectors  $v_i$  corresponding to these small values of  $\lambda_i$  have very little effect upon the calculated radiance at the top of the atmosphere. Thus, these eigenvectors correspond to details of the solution which are easily hidden by a very small amount of noise. Furthermore, it is clear from equation (37) that inclusion of the small eigenvalues associated with these eigenvectors can cause instability or unrealistic results. Therefore, the obvious solution is to truncate the terms containing these components. The problem is to determine how many terms can be carried in the summation of equation (37) with realistic errors added to the measured radiances and to various quantities in equation (1). It is desirable to carry as many terms as possible since, when a term is dropped, ozone information is also lost. There is a trade-off involved between an improved solution due to a decrease in noise sensitivity and a degraded result due to loss of information. This is discussed further in the next section. The number of terms which can be carried that still allow a physically realistic solution is, by definition in this report, the number of independent pieces of information available from the measurements. The types and magnitudes of errors used to determine this information and the responses of the solution to these errors are discussed in the subsequent paragraphs.

#### ERROR STUDY

The "measured" radiances for the error study were calculated with use of equation (1) by assuming a clear sky and by using vertical ozone and temperature distributions measured by the Air Force Cambridge Research Laboratories (refs. 54, and 59 to 61).<sup>3</sup> The Planck radiance at the temperature of the ground was used in computing the effective lower boundary emission, and the surface emissivity was assumed to be 1.0. Transmittances used in the computations were determined with the random exponential band model. The calculations were limited to the spectral range of  $1044 \text{ cm}^{-1}$  to  $1070 \text{ cm}^{-1}$  since this is the region where, currently, the absorption-line parameters are known with the greatest accuracy. (Refer to fig. 2.) Radiances were calculated at nine wave-number centers spaced  $3 \text{ cm}^{-1}$  apart. After computing the "measured" radiances, these values were used to invert equation (1) to obtain ozone information. This procedure gave complete control over all input errors. The "measured" radiances were known perfectly since calculations with equation (1) in the inversion procedure were done in exactly the same way as they

---

<sup>3</sup> These observations were made in situ from a high-altitude balloon at 12 stations covering a latitude range extending from the Canal Zone ( $\approx 9^\circ \text{ N}$ ) to Greenland ( $\approx 77^\circ \text{ N}$ ). The ozone measurements were made with chemiluminescent-type ozonesondes developed by Regener (refs. 62 and 63). The ozone profile above the maximum balloon altitude is determined in this study by extrapolation assuming a constant ozone mixing ratio.

were done when the synthetic radiances were originally computed. Convergence criteria for these computations were applied to the three perturbation parameters  $\Delta p(\text{O}_3)_m$ ,  $\Delta p_m$ , and  $\Delta H$ . The iteration was stopped when the following conditions were met simultaneously:  $\Delta p(\text{O}_3)_m \leq 1 \mu\text{mb}$ ,  $\Delta p_m \leq 1 \text{mb}$ , and  $\Delta H \leq 0.01$ . These limits were selected to give sufficient accuracy in a minimum of computing time. If convergence was not achieved after nine iterations, the initial guess was altered and the procedure was repeated.

The first series of tests was to evaluate the information content of the radiance measurements. Normally distributed random noise was imposed on the "measured" radiances, and inversions were performed for various standard deviations  $\sigma$  of the noise. The calculations showed that it was not possible to obtain realistic solutions when three eigenvectors were included in the expansion of equation (33), even when the radiance noise was as low as  $\sigma = 1$  percent. But when the third eigenvector was truncated, the inversion was very stable and it gave physically possible solutions for noise as large as  $\sigma = 5$  percent. It can be concluded, based on these results, that there are, at most, two pieces of independent information available from the measurements. However, it is still necessary to show that it is always best to use two terms in the expansion; it may be better to use only one term if the noise level is very high since, as indicated in the analysis section, successive truncation of terms continually reduces the sensitivity of the inversion method to noise. Also, if there are two pieces of independent information available, the form of this information must be determined. Both of these tasks were accomplished by performing inversions with all input errors equated to zero for various sets of "measured" radiances. These calculations were done by using radiances determined for 10 different ozone profiles covering the latitude range from  $9^\circ \text{N}$  to  $76.5^\circ \text{N}$ .

The inversion results showed that in order to obtain physically realizable solutions no fewer than two terms should be used in the expansion. Thus, under favorable conditions, there are two pieces of independent information available from the measurements. Furthermore, those two pieces of information are the total ozone  $u$  and the altitude  $h_m$  of the maximum in the profile. The data supporting these conclusions are presented in table I. Table I shows errors in the total ozone and in the altitude of the maximum of the ozone profile when one, two, and three eigenvectors are used in the expansion of equation (35). There is very little change in the root-mean-square errors for the 10 profiles when two eigenvectors are used rather than three, but there is a drastic change in going from two eigenvectors to one. In this latter case, the error in  $u$  goes from 0.95 percent to 28.8 percent and the error in  $h_m$  goes from 0.86 km to 3.1 km. It is clear that the second eigenvector contains so much information that it cannot be discarded even if the noise level is unusually high. The data of table I are explicit examples of the trade-off between reduction of noise sensitivity and loss of information when terms of equation (35) are truncated. Very little information about  $u$  and  $h_m$  is lost when the third eigen-

vector is truncated as shown by the small changes in the root-mean-square errors. Yet, the random-noise study showed that when the third eigenvector is included, the inversion is so sensitive to noise that the solution becomes unstable even for small errors. Therefore, this component should clearly be dropped. On the other hand, a great deal of information is contained in the second eigenvector term and it obviously cannot be neglected.

The inferred ozone information cannot be expressed explicitly in terms of the three parameters of Green's ozone function given by equation (26). The inversion gives one of these parameters,  $p_m$  or  $h_m$ , but the other piece of information is a function of all three parameters through an integral relationship; that is, the total ozone is expressed as

$$u \propto \int_0^{p_s} \frac{p(O_3)}{p} dp \quad (38)$$

where  $p(O_3)$  is the ozone partial pressure,  $p$  is the pressure, and  $p_s$  is the pressure at the surface of the earth.

TABLE I.- ERRORS IN TOTAL OZONE  $u$  AND IN ALTITUDE  $h_m$  OF MAXIMUM OZONE PARTIAL PRESSURE WHEN ALL INPUT ERRORS ARE ZERO

Location	Date of sounding used	Error in $u$ , percent, with -			Error in $h_m$ , km, with -		
		$v_1 + v_2 + v_3$	$v_1 + v_2$	$v_1$	$v_1 + v_2 + v_3$	$v_1 + v_2$	$v_1$
Albrook Fld., Canal Zone (9° N)	7/28/65	-1.3	-0.68	58.0	-0.8	0.1	4.8
	11/18/64	-1.9	-.78	44.6	-.3	.7	4.5
Fla. St. U., Florida (30.4° N)	4/21/65	-1.4	-0.72	12.0	0.5	0.6	1.6
	1/11/65	-1.2	.61	37.1	.4	.7	2.8
Green Bay, Wisconsin (44.5° N)	3/15/65	0.44	1.2	-5.0	0.75	0.8	0.3
	2/18/65	1.2	-.87	-7.7	.6	.2	-.5
Ft. Churchill, Canada (58.8° N)	3/16/65	0.89	2.1	-8.0	0	0.2	-0.2
	9/2/64	-.67	-.55	26.2	.95	.95	4.1
Thule, Greenland (76.5° N)	5/19/65	1.3	-0.3	-0.1	2.8	2.0	3.1
	10/7/64	-.22	.09	23.7	2.3	.7	3.8
Root-mean-square errors		1.15	0.95	28.8	1.27	0.86	3.1

Since the errors of table I were generated with all input errors equal to zero, these errors are the smallest possible values when Green's function is used to model the ozone profile. The errors occur because of the mismatch between Green's function and the atmospheric ozone profiles and because of the small amount of information in the measured radiances. The actual distribution and the profile determined by inversion using two eigenvectors with all errors equated to zero are compared for the July Canal Zone

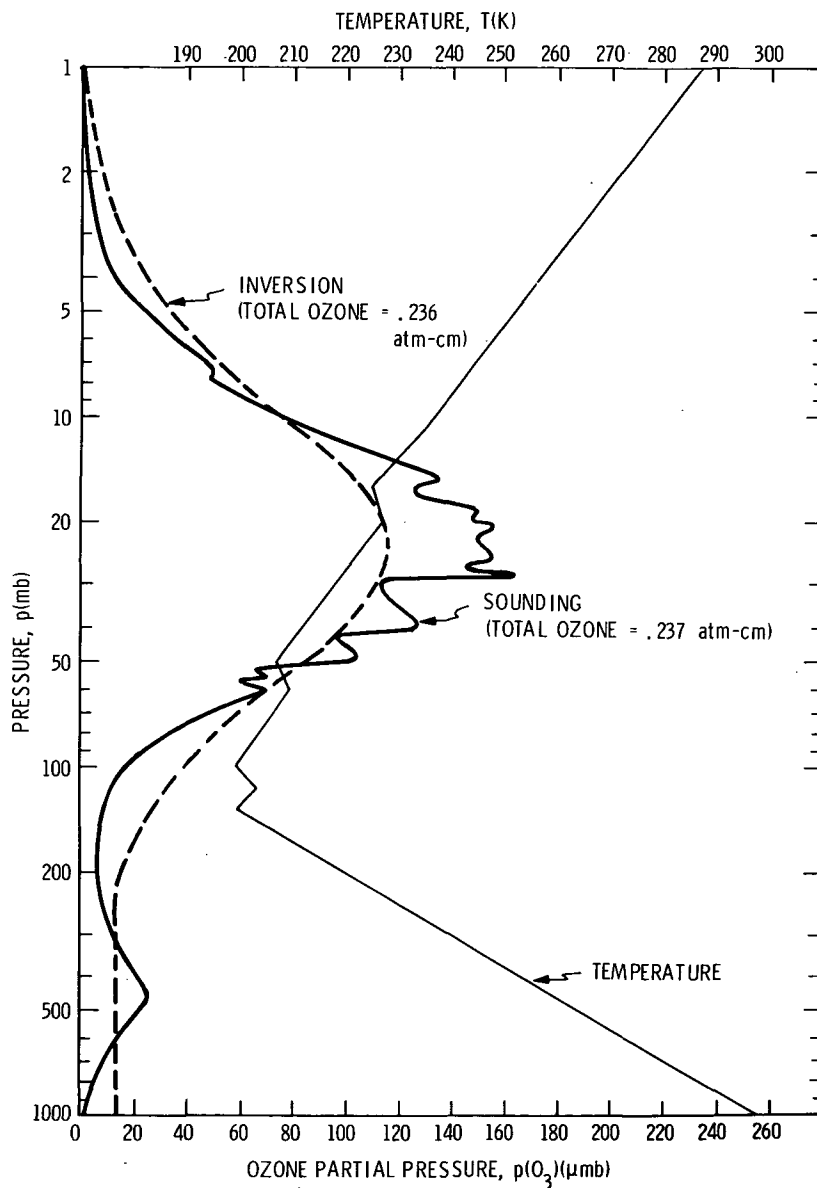


Figure 5.- Comparison of the actual and inferred ozone profiles for a July Canal Zone sounding. All input errors equal zero.

(Albrook Field) sounding and the March Canada (Fort Churchill) sounding in figures 5 and 6, respectively. These results are typical of solutions obtained for the 10 profiles included in this study. The ozone soundings used for figures 5 and 6 were selected because they include opposite extremes of latitude, season, and ozone amount.

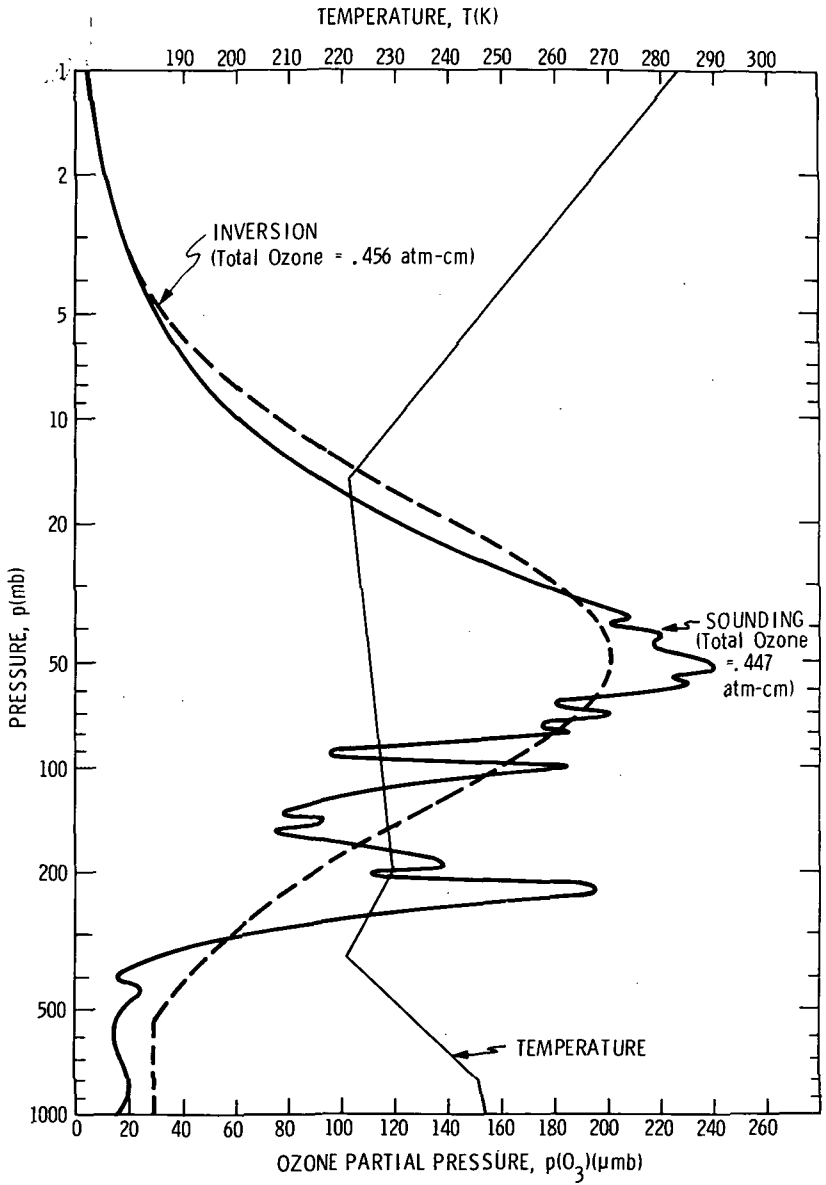


Figure 6.- Comparison of the actual and inferred ozone profiles for a March Canada sounding. All input errors equal zero.

The remainder of the error study was done with two eigenvectors in the expansion. In the next series of tests, individual errors were imposed one at a time. The types and ranges of errors used in these calculations are given in table II. The types of errors in table II are those which probably would be encountered in an actual experiment. The ranges were selected to facilitate unambiguous identification of the most important error effects. The results are presented in figures 7 to 15 for the July Canal Zone profile and the March Canada profile. The errors in  $u$  and  $h_m$  from table I have been subtracted from the errors in each figure. The only errors plotted for  $h_m$  are those due to random radiance noise, lower boundary temperature errors, and temperature-profile bias errors. The effects on  $h_m$  resulting from the remaining types of errors were not plotted since the deduced values were very small ( $\leq 0.4$  km).

The error results show a relatively small latitudinal dependence. The errors which have the greatest effect on the error in total ozone are random radiance noise, lower boundary temperature errors, and absorption-line intensity errors. Those which have the greatest effect on  $h_m$  are random radiance noise, lower boundary temperature errors, and temperature-profile bias errors. Fortunately, large temperature bias errors are unlikely to occur in practice since the temperature profiles that would be used would come from a temperature-inversion method like that of Wark and Fleming (ref. 32) which usually gives both positive and negative errors. Also, the other types of errors can be controlled. As was pointed out in the analysis section, the effective lower boundary temperature can be determined to within 0.5 K or less and, undoubtedly, errors in the absorption-line intensities will eventually be improved as work advances to eliminate defects in current theories regarding the ozone molecule. Once the accuracies of the absorption-line intensities are increased, the entire ozone band can be used in the calculations thereby causing a reduction in the effective value of the random radiance noise.

TABLE II.- TYPES AND RANGES OF ERRORS USED IN STUDY OF INDIVIDUAL ERROR EFFECTS IN NADIR EXPERIMENT

Type of error	Range
Random radiance noise, normally distributed with a mean of zero, percent . . .	Standard deviation: <sup>a</sup> $\sigma = 1, 3, \text{ and } 5$
Radiance bias, watts/m-sr . . . . .	$\pm 0.3 \times 10^{-5}$
Temperature profile, alternating sign, kelvins . . . . .	$b_0 \pm 20$
Temperature-profile bias, kelvins . . . . .	$\pm 7$
Ozone absorption-line intensity, percent . . . . .	$\pm 15$
Lower boundary temperature, kelvins . . . . .	$\pm 2$

<sup>a</sup> Fifteen inversions were performed for each value of standard deviation.

<sup>b</sup> This is the maximum difference between the true profile and the error profile at each of six different altitudes in the range from the ground to the stratopause. The errors between any two of these altitudes varied linearly going from a plus value at one level to a minus value at the next.

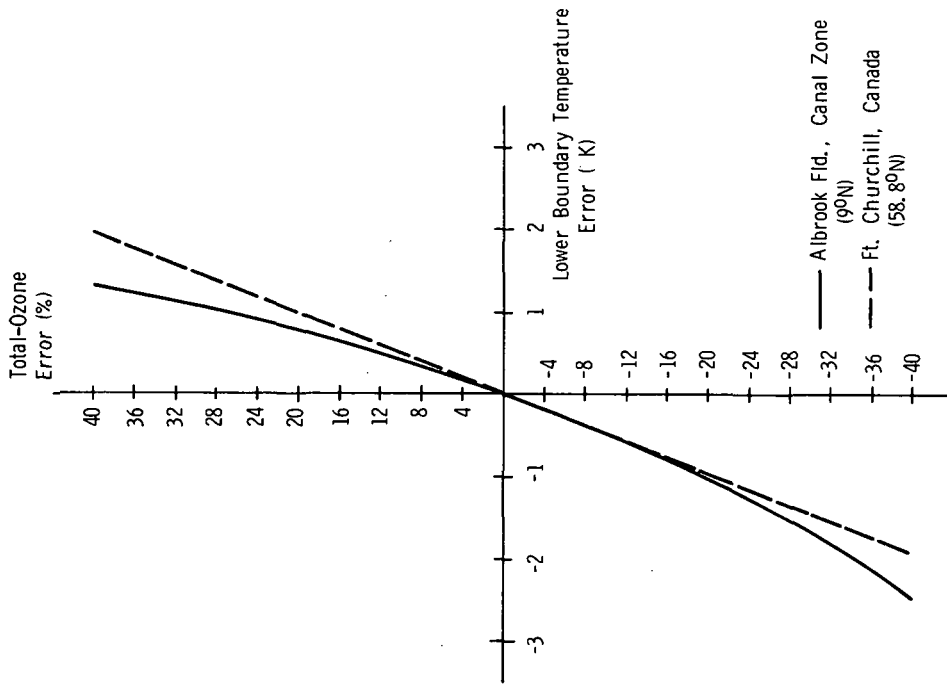


Figure 8.- Total-ozone error plotted against lower boundary temperature error.

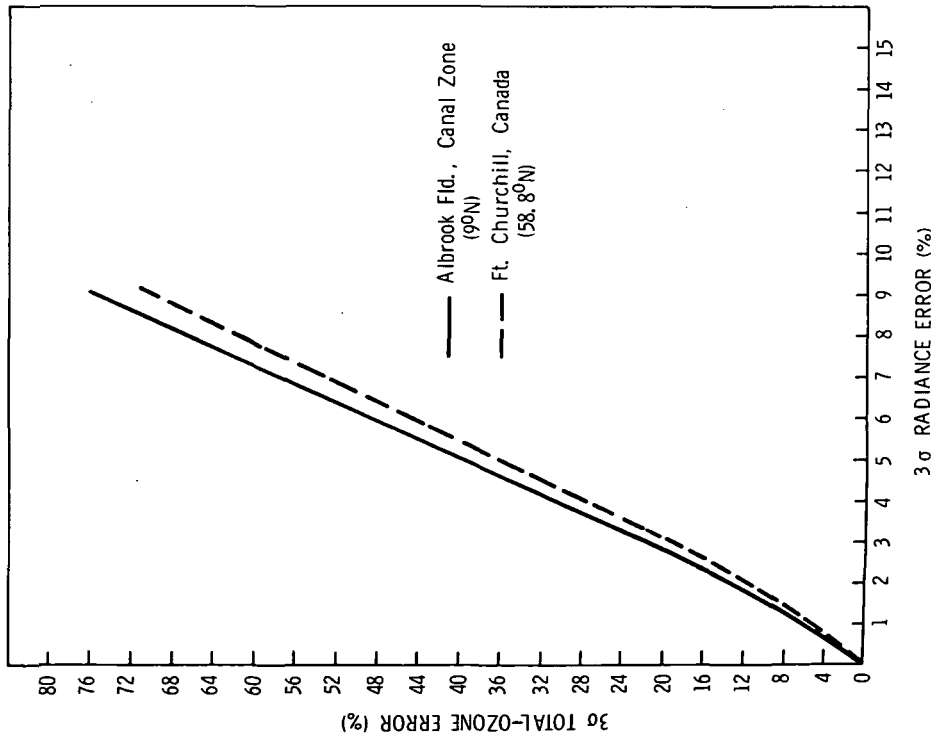


Figure 7.- A 3σ total-ozone error plotted against a 3σ radiance error for normally distributed random radiance noise with a mean of zero.

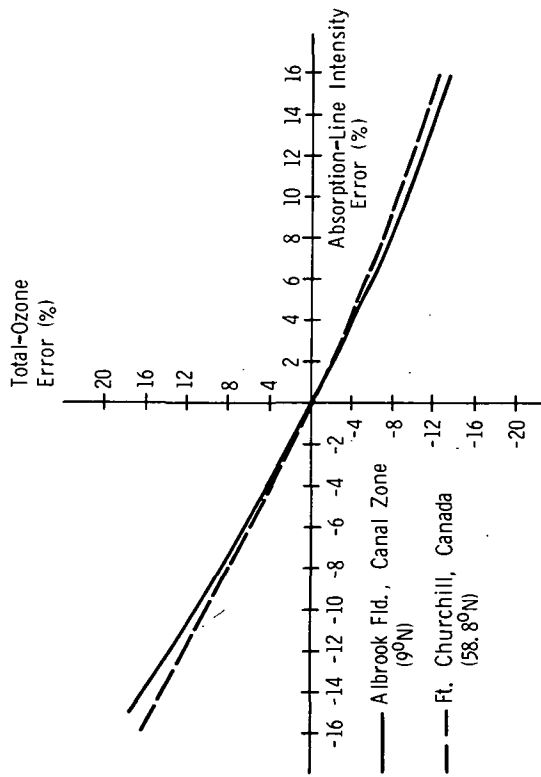


Figure 9.- Total-ozone error plotted against absorption-line intensity error.

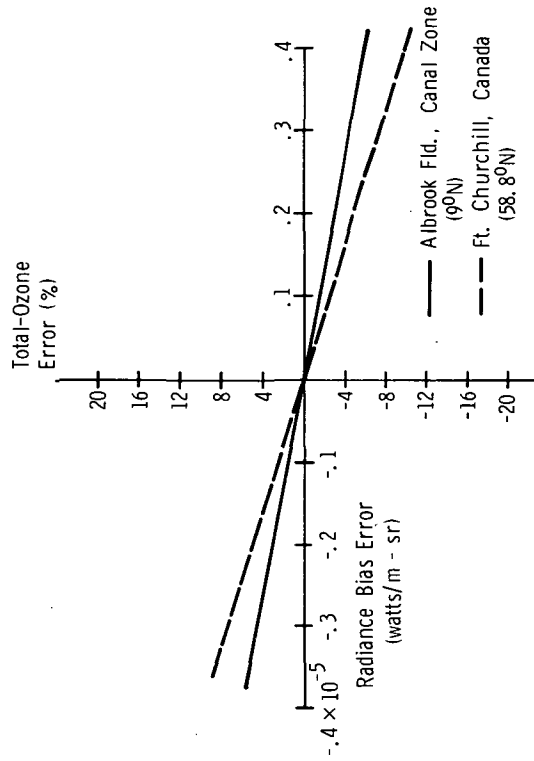


Figure 10.- Total-ozone error plotted against radiance bias error.

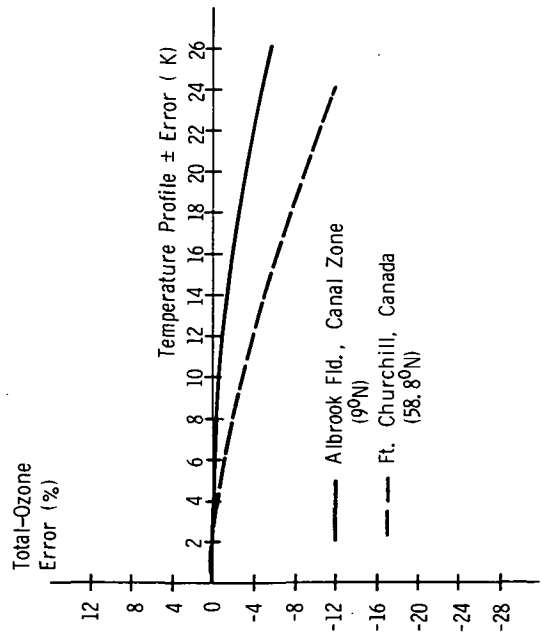


Figure 11.- Total-ozone error plotted against temperature profile ± error.

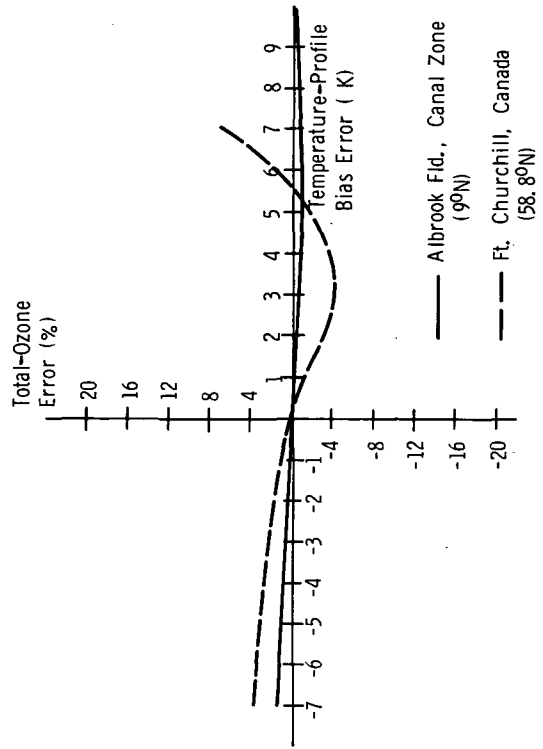


Figure 12.- Total-ozone error plotted against temperature-profile bias error.

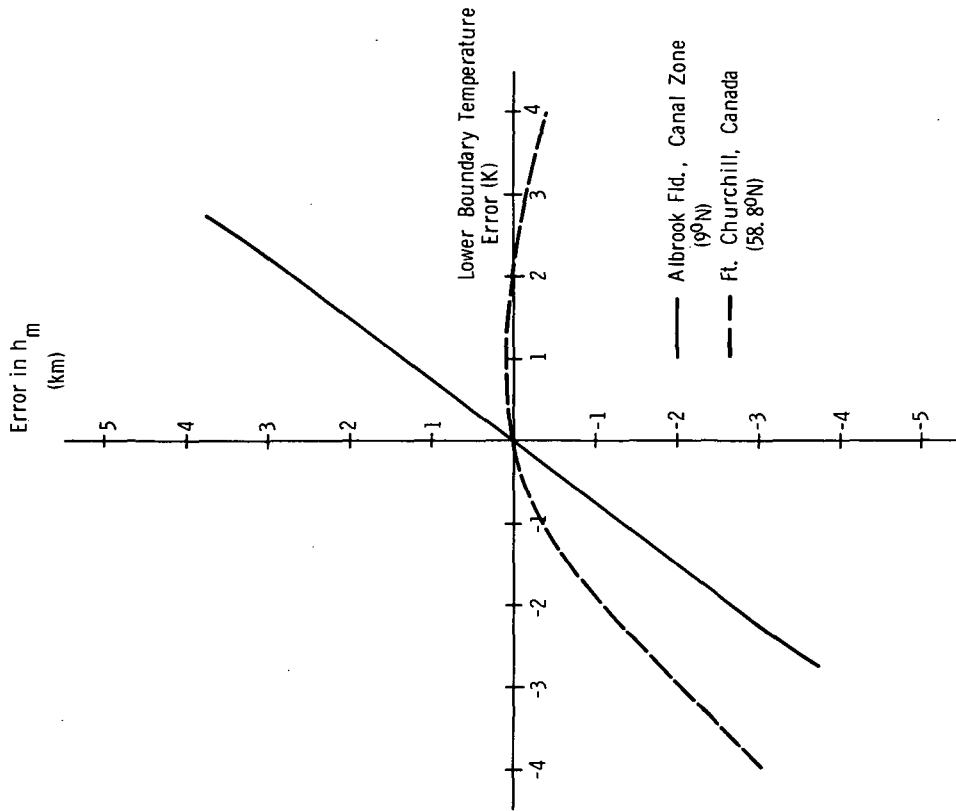


Figure 14.- Error in altitude  $h_m$  of the maximum ozone partial pressure plotted against lower boundary temperature error.

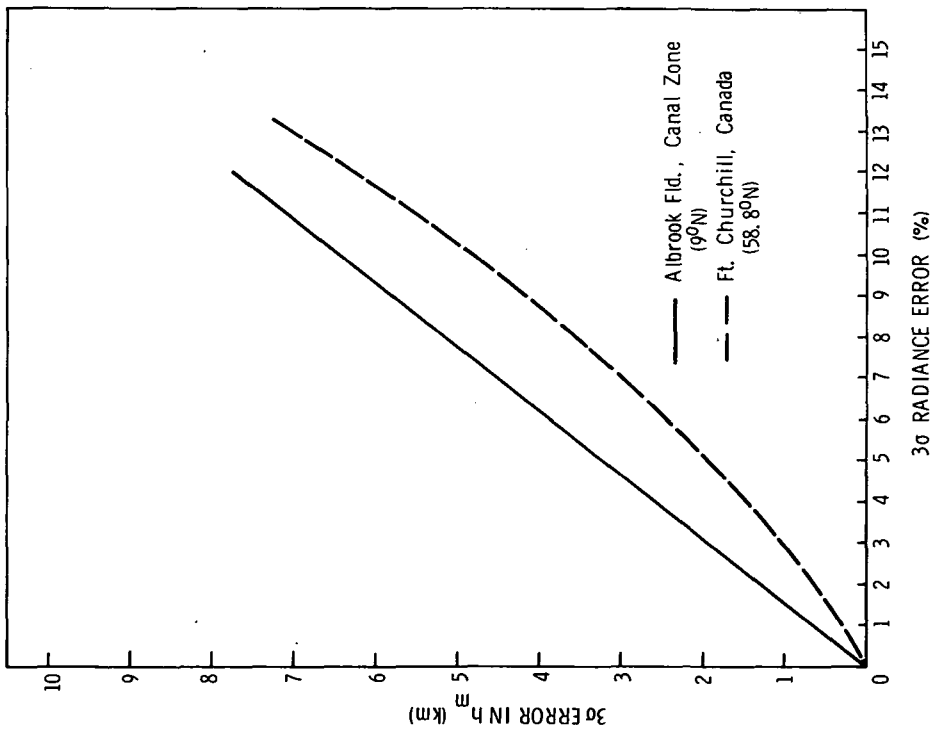


Figure 13.- A  $3\sigma$  error in altitude  $h_m$  of the maximum ozone partial pressure plotted against  $3\sigma$  radiance error for normally distributed random radiance noise with a mean of zero.

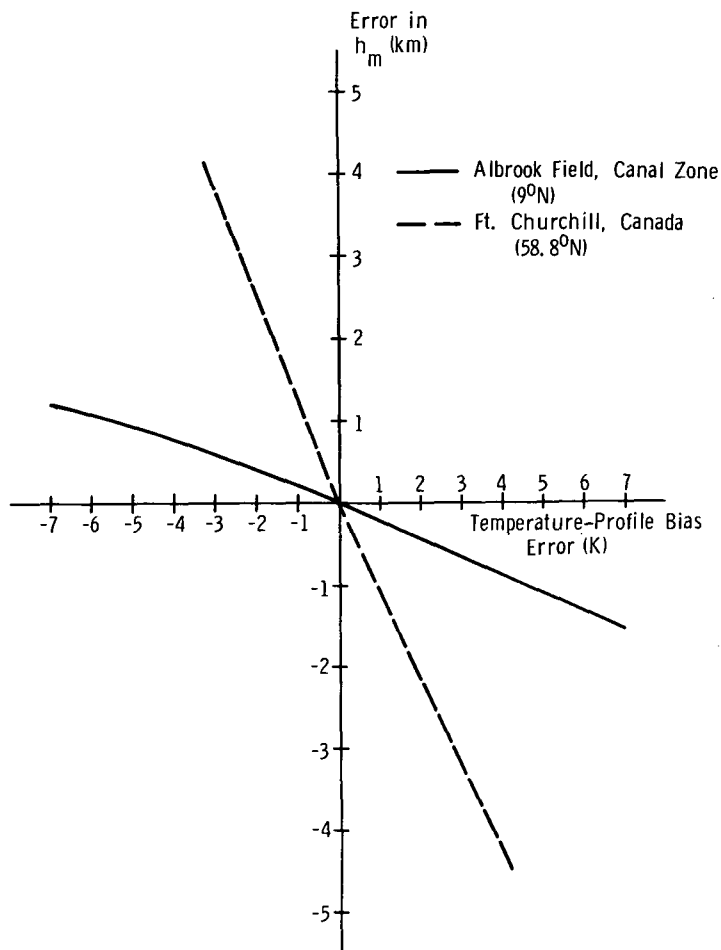


Figure 15.- Error in altitude  $h_m$  of the maximum ozone partial pressure plotted against temperature-profile bias error.

To determine the ultimate accuracy which can be expected for  $u$  and  $h_m$  with the present inversion scheme, the conditions of table III were imposed simultaneously. The best case values in table III contain errors which have canceling effects on each other, and the worst case values contain errors which are all additive in effect. The values represent error limits presently attainable (for the lower boundary temperature and temperature-profile errors) or limits which probably can be achieved in the future. The standard deviation of the radiance noise was selected in the following way: if the standard deviation of the radiance noise is 1 percent, which is currently possible, and if 30 wave numbers can eventually be used (once the accuracies of the absorption-line intensities are improved), then the effective standard deviation can be reduced to  $\sigma_{\text{eff}} = \frac{\sigma}{\sqrt{n}} = \frac{0.01}{\sqrt{30}} = 0.18$  percent. This value can be simulated in the current calculations with  $\sigma = 0.54$  percent, since with nine wave numbers  $\sigma_{\text{eff}} = \frac{0.0054}{\sqrt{9}} = 0.18$  percent. The

TABLE III.- ERRORS USED IN SIMULTANEOUS ERROR STUDY OF NADIR EXPERIMENT

Type of error	Best case values	Worst case values
Radiance noise, percent . . . . .	$\sigma = 0.54$	$\sigma = 0.54$
Radiance bias, watts/m-sr . . . . .	$-0.15 \times 10^{-5}$	$0.15 \times 10^{-5}$
Temperature profile, alternating sign, kelvins . .	$\pm 3$	$\pm 3$
Ozone absorption-line intensity, percent . . . . .	4	4
Lower boundary temperature, kelvins . . . . .	0.4	-0.4

TABLE IV.- ERRORS IN TOTAL OZONE  $u$  AND IN ALTITUDE  $h_m$  OF MAXIMUM OF OZONE PROFILE WHEN ERRORS OF TABLE III ARE IMPOSED SIMULTANEOUSLY

Location and date of sounding used	Best case errors				Worst case errors			
	Error in $u$ , percent		Error in $h_m$ , km		Error in $u$ , percent		Error in $h_m$ , km	
	Mean	Std. dev.	Mean	Std. dev.	Mean	Std. dev.	Mean	Std. dev.
Albrook Fld., Canal Zone (9° N) 7/28/65	3.4	4.7	0.17	0.3	-16.0	3.5	-1.0	0.4
Ft. Churchill, Canada (58.8° N) 3/16/65	6.7	3.4	0.15	0.16	-14.3	3.4	0.28	0.2

remaining quantities of table III are estimates of final accuracies. The resulting errors are given in table IV. The mean error in total ozone ranges from 3.4 percent in the best case to -16 percent in the worst case with a standard deviation of about 4 percent. Thus, it is not unreasonable to expect that total ozone can eventually be determined to within 10 percent or less. Also, the error in  $h_m$  varies from 0.15 km in the best case to -1 km in the worst case with a standard deviation of approximately 0.3 km. It would appear that this parameter can ultimately be determined to within about 0.5 km. However, some caution should be exercised here since table I shows several errors in  $h_m$  which are greater than 0.5 km even when all input errors are zero. The "all error"

study indicates such small discrepancies because the two ozone profiles used in the study were matched reasonably well by Green's ozone function (eq. (26)), thereby giving a small "zero error" for  $h_m$  in both cases. This will not always be true as table I shows. However, it is reasonable to expect, based on tables I and IV, that  $h_m$  can be determined to within about 1.5 km, at least for the large majority of profiles encountered in the atmosphere.

The calculations of table IV were repeated for varying degrees of cloudiness in the troposphere. To simulate the effect of clouds, the effective lower boundary emission was computed by weighting emissions from the ground and cloud tops according to the percentage cloud cover.<sup>4</sup> The clouds were considered to be black, and the Planck radiance  $B_{eff}$  of the effective lower boundary was computed according to the equation

$$B_{eff} = B_{gnd}(1 - P_{cL}) + B_{cL} P_{cL} \quad (39)$$

where  $B_{gnd}$  is the Planck radiance at the ground temperature,  $B_{cL}$  is the Planck radiance at the cloud-top temperature, and  $P_{cL}$  is the percentage cloud cover. Altostratus cloud covers of 100 percent and 8 percent at 5 km were used for the Canal Zone, and values of 100 percent and 12 percent at 3 km were used for the Canada calculations. These conditions, exclusive of the complete cloud covers, are averages for the respective locations according to data published by London (ref. 64). The calculations revealed only a small effect due to the presence of clouds. Negligible changes occurred in the errors of table IV when partially cloudy conditions were used, and the errors increased only slightly when a complete cloud cover was used. The means and standard deviations of the errors in  $u$  increased by about 2 to 3 percent, and the errors in  $h_m$  increased about 0.2 km. Therefore, it appears that the presence of clouds will not seriously degrade the inversion results as long as there is some contrast between the ozone spectrum and the effective lower boundary emission spectrum. (See appendix B.)

Since the band model used in the error study did not allow for variation in absorption-line intensity with temperature, a test was conducted to evaluate this effect. The line-by-line integration technique was used to compute the atmospheric transmittances for a mid-latitude ozone profile and a corresponding temperature profile. This was done for the reference temperature profile and for a profile 10 K higher in temperature at every point. These two sets of transmittances were then used along with the reference temperature profile and equation (1) to compute the radiances at the top of the atmosphere. The results are plotted in figure 16. The computations show a slight temperature dependence, mostly in the wings of the ozone band, but the effect is so small that it would not change the results of the error study significantly if it were included in the calculations.

---

<sup>4</sup>The percentage cloud cover is not required in applying the inversion technique to flight data since cloud effects are treated indirectly by the method discussed in the analysis section.

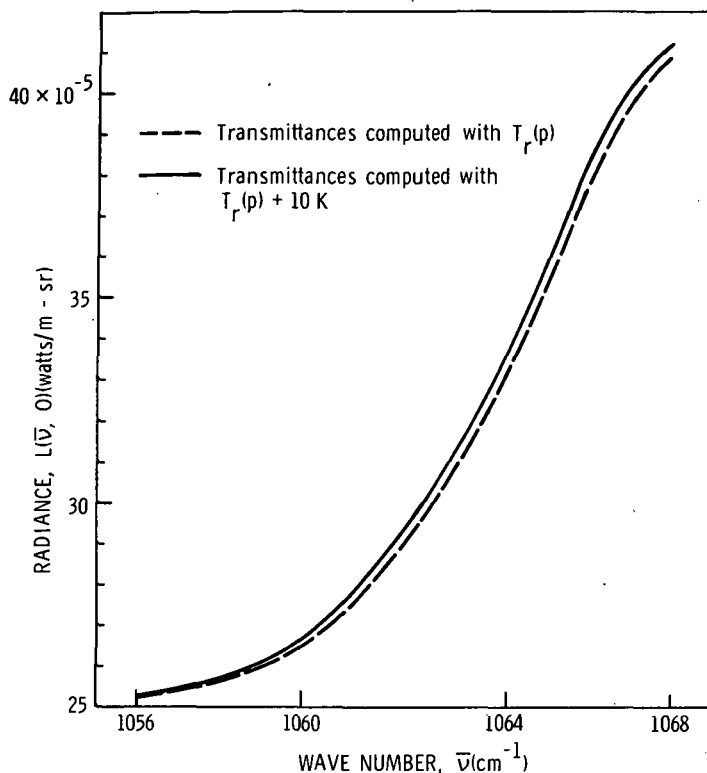


Figure 16.- Effect of temperature on the ozone spectrum. Dashed curve computed by using reference temperature profile  $T_r(p)$ . Solid curve computed by using reference temperature profile plus 10 kelvins.

The inferred values of  $u$  and  $h_m$  would differ by about 8 percent and 0.4 km, respectively, for the two spectra of figure 16. This effect is large enough that it should not be neglected in precise calculations such as when applying the inversion method to actual radiances measured from a balloon or satellite.

## APPLICATIONS

### Palestine, Texas, Data

The analysis methods were applied first to radiances measured from a balloon at the 31-km level above Palestine, Texas (31.8° N, 96° W). The measurements were made on May 8, 1966, in a flight conducted by the High Altitude Engineering Laboratory of the University of Michigan. The instrumentation and other details concerning the flight have been discussed in a report by Chaney et al. (ref. 29). A breadboard version of an IRIS having a resolution of 5  $\text{cm}^{-1}$  was used to make the radiance measurements, and a typical spectrum from the experiment was presented in figure 1.

The data were of very good quality. The standard deviation of the radiance noise was only  $0.5 \times 10^{-5}$  watt/m-sr which corresponds to a level of about 1.3 percent in the center of the ozone band and less than 1 percent in the wing region. This low noise made the data especially well suited to test the inversion method. Unfortunately, neither the total ozone nor the vertical ozone distribution was measured at the time and location of the balloon. Therefore, it was not possible to make a direct comparison between measured quantities and values determined from the inversion. However, the total ozone could be estimated for Palestine based on a Dobson measurement made at Albuquerque, New Mexico ( $35^{\circ}$  N,  $106.6^{\circ}$  W). According to H. S. Muench of the Air Force Cambridge Research Laboratories, the ozone amount at Albuquerque on the day of the balloon flight was 0.317 atm-cm, and since Palestine, Texas, is located at a slightly lower latitude, the total ozone there should have been slightly less; a reasonable guess would be a value of 0.298 atm-cm. This estimate is based on a total-ozone latitudinal gradient of 0.006 atm-cm per degree of latitude as determined from data presented by Hering and Borden (ref. 61). There was no vertical sounding at Albuquerque on the day of the balloon flight which could be used to estimate the altitude of the primary maximum in the ozone profile. Past measurements at the same time of year at Albuquerque indicate that the value of  $h_m$  could lie anywhere in the range from about 23 km to 27 km.

Transmittances used in the inversions were calculated by the line-by-line method rather than by the less accurate random-exponential-band-model approach. Inversions were attempted by using the radiances of table V and the atmospheric temperature profile measured in situ from the balloon. A stable solution could be obtained only after water-vapor line absorption was neglected in determining the lower boundary emission. This was equivalent to using background radiances which were too high; that is, it was equivalent to having a positive error in the lower boundary temperature. The most likely reason that the higher background emission was needed was that it compensated for a positive absorption-line intensity error. Figures 8 and 9 show that positive errors in the lower boundary temperature and the absorption-line intensity have canceling effects on each other. A positive absorption-line intensity error should be expected based on figure 2 which shows that there is too much calculated absorption over the spectral range of table V for a homogeneous path. Other calculations with the Nimbus data also show that this is true for an atmospheric path.

The theory of canceling error effects is plausible when estimates of the errors involved are considered. For example, the background radiance error was about  $10^{-5}$  watt/m-sr in the wings of the band. This corresponds to a lower boundary temperature error of about 1 K. According to figure 8, a 1 K error, causes a total-ozone error of about 25 percent. The error in absorption-line intensity can be estimated from figure 1. A representative error for the interval of table V is about 35 percent. If the curve of figure 9 is extrapolated, it shows that a 35-percent error causes a total-ozone

error of around -30 percent. When the two sources of error are combined, the net result is a total-ozone error of only about -5 percent.

TABLE V.- PALESTINE, TEXAS, DATA

Wave number, $\text{cm}^{-1}$	Radiance, $\bar{L}(\bar{\nu}, 0)$ , watts/m-sr
1052	$37.2 \times 10^{-5}$
1056	38.6
1060	45.2
1062	50.3
1066	61.5
1068	66.8
1070	70.8

There was almost complete cancellation of error effects for the spectral range of  $1060 \text{ cm}^{-1}$  to  $1070 \text{ cm}^{-1}$  where the absorption-line intensity error was large and positive. However, this was not true for the remaining region of table V ( $1052 \text{ cm}^{-1}$  to  $1060 \text{ cm}^{-1}$ ) where the absorption-line intensity errors were different. Figure 2 shows that the absorption errors are smaller in the range of  $1052 \text{ cm}^{-1}$  to  $1060 \text{ cm}^{-1}$  and the error changes sign; at  $1052 \text{ cm}^{-1}$  the error is almost zero and it is negative. Thus, when the wave numbers centered at  $1052 \text{ cm}^{-1}$  and  $1056 \text{ cm}^{-1}$  were included in the calculations, the balance of error effects was upset. The effect of using these wave numbers was to cause the computed spectrum to shift upward in the wing region of the band. The shift was due to a change in slope of the spectrum in the wing region brought about by the least-squares fitting procedure. The slope became progressively steeper as first  $1056 \text{ cm}^{-1}$  and then  $1052 \text{ cm}^{-1}$  was included. The steeper slope gave higher radiances at every point which corresponded to less ozone absorption and, hence, smaller ozone amounts. For example, when all wave numbers of table V were used, the inverted ozone amount was  $0.129 \text{ atm-cm}$ ; when the  $1052 \text{ cm}^{-1}$  wave number was dropped, the value of inferred total ozone increased to  $0.161 \text{ atm-cm}$ . Finally, when both wave numbers were dropped to give good cancellation of error effects, the value of inferred total ozone increased to  $0.294 \text{ atm-cm}$ . Since the balloon was not at the top of the atmosphere, this value should be increased by about 5 percent to account for the ozone above the balloon. When this is done, the inferred total ozone becomes  $0.309 \text{ atm-cm}$ . This is in excellent agreement with the value estimated for Palestine, Texas. The Green ozone function (eq. (24)) corresponding to this inversion is shown in figure 17. The value of  $h_m$  is  $26.6 \text{ km}$  which is within the expected range of values for the latitude and time of year of the measurement. These results, coupled with the results of the error study, prove the validity of the inversion method developed in the analysis section.

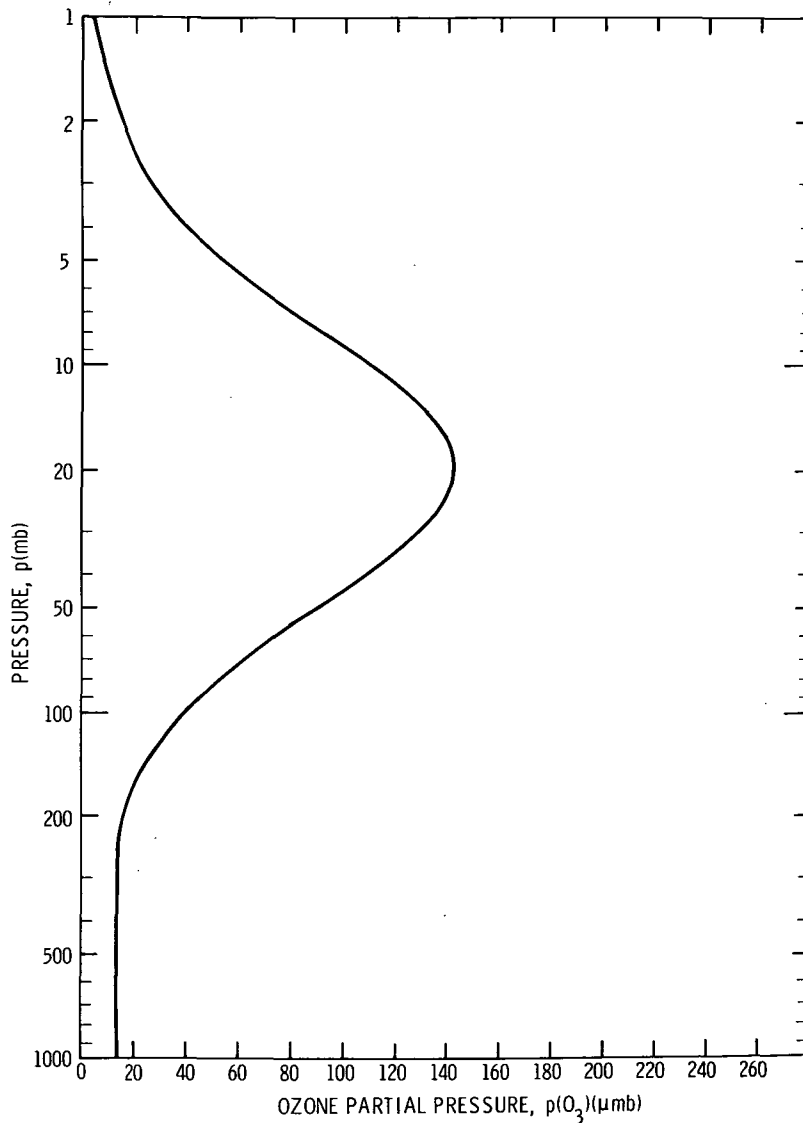


Figure 17.- Ozone profile inferred by using radiances measured from a balloon above Palestine, Texas, on May 8, 1966.

The results also suggest a need for further work to increase the accuracy of the absorption-line intensities. Because of the low noise level in the Palestine radiances, it was possible ultimately to perform the inversion by using only five wave-number centers in a narrow spectral interval ( $1060\text{ cm}^{-1}$  to  $1070\text{ cm}^{-1}$ ). With this narrow interval, a cancellation of error effects due to absorption-line intensity errors was obtained by adding positive background radiance errors. However, such a narrow interval will not afford enough suppression of random radiance noise to permit accurate results for noise levels normally encountered (this is vividly illustrated in later calculations with the Nimbus III data); and when a wider interval is used to reduce the effective noise level, error effects

no longer cancel because of the change in algebraic sign of the absorption error in one-half of the band. This illustrates the need for more accurate values of the absorption parameters across the band.

### Nimbus Data

The solution procedures were also applied to radiances measured by an IRIS mounted on the Nimbus III satellite launched in April 1969. These data were kindly provided to the author by B. J. Conrath of the Goddard Space Flight Center. The location of the subsatellite point at the time of the measurements was 20.8° N, 70.9° W. This is very close to the Grand Turk Air Force Base (21.5° N, 71.1° W) where an ozonesonde observation was made less than 24 hours before the satellite pass. Since daily ozone variations are quite small in the temperate zone, the ozone profile probably changed only slightly between the time of the ozonesonde launch and the time that the radiances were measured. Therefore, the ozonesonde data should be a good gage for evaluating the inversion results.

Unfortunately, the Nimbus III measurements were of poor quality in the vicinity of 1042 cm<sup>-1</sup>. The noise-equivalent radiance was about  $2 \times 10^{-5}$  watt/m-sr (ref. 28). This corresponds to an error of about 5 percent in the center of the ozone band and of approximately 3 percent in the wing region. Considering the mean error to be 4 percent gives a  $3\sigma$  radiance error of 12 percent; and, according to figures 7 and 13, this causes a  $3\sigma$  total-ozone error of about 96 percent and a  $3\sigma$   $h_m$  error of about 7.7 km. Therefore, it is anticipated that inversion results using the Nimbus data will be poor.

Inversions were performed by using the data of table VI and the temperature profile measured in situ at the time of the ozonesonde observations. The first inversion was attempted by using background radiances that included water-vapor line absorption and, as with the Palestine data, the solution was unstable. Therefore, water-vapor line absorption was neglected for the same reason as was discussed in the previous subsection.

TABLE VI.- NIMBUS DATA

Wave number, cm <sup>-1</sup>	Radiance, $\bar{L}(\bar{\nu}, 0)$ , watts/m-sr
1053.3	$40.3 \times 10^{-5}$
1055.4	42.1
1059.5	45.4
1061.6	49.0
1065.8	56.4
1067.9	59.5
1070.0	60.2

When wave numbers less than a value of about  $1060 \text{ cm}^{-1}$  were used, the solution was also unstable. This was probably due to the combined influence of the high-radiance noise and the imbalance of error effects brought about by absorption-error differences in the spectral region below  $1060 \text{ cm}^{-1}$  (as discussed in the previous subsection). Finally, an inversion was performed by using the same spectral range as was ultimately used with the Palestine data and the solution was barely stable. It did not converge until the seventh iteration. Usually, convergence is achieved in only three or four iterations. The inversion gave a total-ozone value of  $0.062 \text{ atm-cm}$  and a value for  $h_m$  of  $18.7 \text{ km}$ . These correspond to errors of  $-76$  percent and  $-6.3 \text{ km}$ , respectively, which, as expected, are large errors. The error magnitudes are consistent with the values predicted from figures 7 and 13. These results could be improved by using the entire ozone band to reduce the effective noise level, but as previously discussed, existing absorption errors prohibit this.

In order to evaluate typical absorption errors for an atmospheric path, the radiance at the top of the atmosphere was computed by using ozonesonde and temperature data taken at Grand Turk. Water-vapor line absorption was considered in computing the background radiances, and the line-by-line technique was used to compute the transmittances. Computed values were compared to the radiances measured at the satellite and the results are shown in table VII. The quantity  $\Delta L = \bar{L}_{mi} - \bar{L}_{ci}$  is the difference between the measured and calculated radiances. Table VII shows that there is too much calculated absorption in the region of  $1060 \text{ cm}^{-1}$  to  $1070 \text{ cm}^{-1}$  for the atmospheric path just as it is for the homogeneous path spectrum shown in figure 2. This supports the argument of the previous subsection that justified the need for positive background radiance errors because of the presence of positive absorption-line intensity errors.

TABLE VII.- DIFFERENCES BETWEEN RADIANCES MEASURED ON-BOARD NIMBUS III AND RADIANCES COMPUTED BY USING CORRESPONDING OZONE PROFILE

Wave number, $\text{cm}^{-1}$	Radiance difference, $\Delta L$ , watts/ $\text{m}^2\text{-sr}$
1053.3	$-1.6 \times 10^{-5}$
1055.44	.33
1059.5	1.5
1061.6	4.1
1065.8	4.7
1070	1.4

## CONCLUDING REMARKS

A workable technique has been developed for inverting nadir measurements to obtain ozone information. The success of the method depends critically on the accuracy of the quantity which represents the energy emitted from the lower boundary under a satellite. A method was formulated for computing this quantity which circumvents the troublesome problems caused by the water-vapor continuum absorption and by atmospheric clouds. By incorporating water-vapor line absorption in the calculations, the effective temperature of the lower boundary could be found to within 0.5 K or less. The inversion equations were expanded in terms of the eigenvectors and eigenvalues of a least-squares-solution matrix, and an analysis was performed by using synthetic clear-sky radiances computed for 10 different ozone profiles. The results showed that, under favorable conditions, infrared radiance measurements in the ozone band contained two pieces of independent information: the total ozone  $u$  and the altitude  $h_m$  of the primary maximum in the ozone profile. It is not possible to obtain the value of the maximum ozone partial pressure or the width of the ozone profile from these data. A comprehensive study, using a variety of error sources, revealed that errors in  $u$  are most sensitive to random radiance errors, lower boundary temperature errors, and ozone absorption-line intensity errors. Errors in  $h_m$  are affected most by the former two errors and by temperature-profile bias errors.

In the next series of tests, all error sources were considered simultaneously. The results showed that it should ultimately be possible to determine  $u$  to within 10 percent or less and to determine  $h_m$  to within 1.5 km when the root-mean-square radiance noise level is 1 percent or less. These calculations were also made for varying degrees of cloudiness in the troposphere. The data showed that the presence of clouds does not seriously affect results as long as there is some contrast between the ozone spectrum and the effective lower boundary emission spectrum. Sometimes, in high-latitude areas of the globe, there may be little or no contrast between these spectra due to the effects of temperature profile and cloud conditions. Under these circumstances, it may be difficult or impossible to infer ozone information from the measurements.

Finally, the inversion technique was applied to balloon data measured over Palestine, Texas, and to the Nimbus III satellite data measured over Grand Turk Island in the Bahamas. The two sets of measurements were in sharp contrast with each other; the balloon data contained very little noise, whereas the satellite data were very noisy by comparison. The inversion results reflected this contrast. The Palestine inversion was satisfactory considering the uncertainties which existed. The errors in  $u$  and  $h_m$  were estimated to be well within the limits of 10 percent and 1.5 km, respectively. However, the Nimbus results were poor. The total ozone  $u$  was off by 76 percent and  $h_m$

was in error by 6.3 km. If absorption errors throughout the band had been smaller, the Nimbus results could have been substantially improved by using the entire ozone band to reduce the effective radiance noise level. Unless absorption-line intensities are improved by empirical or other methods, calculations will have to be limited to a narrow spectral interval and, consequently, to low-noise data (less than 1 percent).

Langley Research Center,  
National Aeronautics and Space Administration,  
Hampton, Va., February 13, 1973.

## APPENDIX A

### RELATIONSHIPS FOR THE RANDOM EXPONENTIAL BAND MODEL AND THE CURTIS-GODSON APPROXIMATION

The transmittance through a homogeneous layer is given by Goody (ref. 42) as

$$\overline{\tau(\bar{\nu}, \bar{p}_k)} = \exp \left\{ - \frac{(\beta_{\bar{\nu}}/d) \bar{u}_k}{\left[ 1 + 2 \left( \frac{\beta_{\bar{\nu}}}{2\pi\alpha_{Lo}(\bar{\nu})} \right) \bar{l}_k \right]^{1/2}} \right\} \quad (A1)$$

and he shows that, in order to force a fit in the weak-line ( $\bar{u}_k \ll 1$ ) and strong-line ( $\bar{u}_k \gg 1$ ) regions, the following expressions should be used:

$$\frac{\beta_{\bar{\nu}}}{d} = \frac{\sum_{i=1}^{N'} S_i}{\Delta\bar{\nu}} \quad (A2)$$

$$\frac{\beta_{\bar{\nu}}}{2\pi\alpha_{Lo}(\bar{\nu})} = \frac{1}{8} \frac{\left[ \sum_{i=1}^{N'} S_i \right]^2}{\sum_{i=1}^{N'} (S_i \alpha_{i0})^{1/2}} \quad (A3)$$

where  $N'$  is the total number of lines in the interval  $\Delta\bar{\nu}$  and  $\alpha_{i0}$  is the Lorentz half-width of the  $i$ th line at standard temperature and pressure.

According to the Curtis-Godson approximation the effective pressure of the atmosphere between the satellite and an arbitrary pressure  $p_0$  is

$$\bar{p}_k = \frac{\int_0^{p_0} p S[T(p)] \frac{q}{g} dp}{\int_0^{p_0} S[T(p)] \frac{q}{g} dp} \quad (A4)$$

## APPENDIX A – Concluded

where  $q$  is the absorber mass mixing ratio and  $g$  is the acceleration of gravity. The effective absorber amount is

$$\bar{u}_k = \frac{\int_0^{p_0} S[T(p)] \frac{q}{g} dp}{S(\bar{T})} \quad (A5)$$

where  $\bar{T}$  is a mean temperature. However, if  $S[T(p)] = S(\bar{T})$ , that is, if the line intensity does not vary with altitude, then equations (A4) and (A5) become

$$\bar{p}_k = \frac{\int_0^{p_0} p \frac{q}{g} dp}{\int_0^{p_0} \frac{q}{g} dp} \quad (A6)$$

$$\bar{u}_k = \int_0^{p_0} \frac{q}{g} dp \quad (A7)$$

The effective length of the homogeneous path is computed by

$$\bar{l}_k = \frac{\bar{u}_k}{\bar{p}_k} \quad (A8)$$

These last three equations, along with equations (A1), (A2), and (A3), are used throughout this report to compute the transmittance when the random-exponential band model is used. The line intensities required to compute equations (A2) and (A3) were taken from Clough and Kneizys (ref. 35). The half-width was considered to be the same for all lines and equal to  $0.08 \text{ cm}^{-1}$  at standard temperature and pressure. This value was suggested by Clough and Kneizys (ref. 35) and used by Goldman and Kyle (ref. 41).

## APPENDIX B

### EFFECT OF LOWER BOUNDARY EMISSION ON THE OZONE SPECTRUM

The energy emitted by the underlying boundary can have a significant effect on the ozone spectrum measured at the top of the atmosphere. Assume, for the present, that the emissivity of the lower boundary is one and that the ozone layer is isothermal at a temperature  $T(p_r)$  which is different from the temperature  $T(p_g)$  of the lower boundary where  $p_r$  is the pressure at the bottom of the ozone layer and  $p_g$  is the pressure at the lower boundary. These conditions are represented in figure 18. In this case equation (1) can be written as

$$\begin{aligned} \overline{L(\bar{\nu}_0, 0)} &= B[\bar{\nu}_0, T(p_g)] \overline{\tau(\bar{\nu}_0, p_g)} - B[\bar{\nu}_0, T(p_r)] \int_1^{\tau(\bar{\nu}_0, p_T)} \overline{d\tau(\bar{\nu}_0, p)} \\ &\quad - \int_1^{\tau(\bar{\nu}_0, p_g)} \frac{\overline{d\tau(\bar{\nu}_0, p)} B[\bar{\nu}_0, T(p)]}{\tau(\bar{\nu}_0, p_T)} \end{aligned} \quad (B1)$$

where  $p_T$  is the pressure at the top of the effective lower boundary. If it is assumed that  $\overline{\tau(\bar{\nu}_0, p_T)} \approx \tau(\bar{\nu}_0, p_g)$ , then equation (B1) reduces to the following after integration:

$$\overline{L(\bar{\nu}_0, 0)} = \left\{ B[\bar{\nu}_0, T(p_g)] - B[\bar{\nu}_0, T(p_r)] \right\} \overline{\tau(\bar{\nu}_0, p_g)} + B[\bar{\nu}_0, T(p_r)] \quad (B2)$$

The spectrum defined by equation (B2) and different values of  $\bar{\nu}_0$  will show the structure of the ozone band because of the factor  $\overline{\tau(\bar{\nu}_0, p_g)}$ . However, if the lower boundary is at

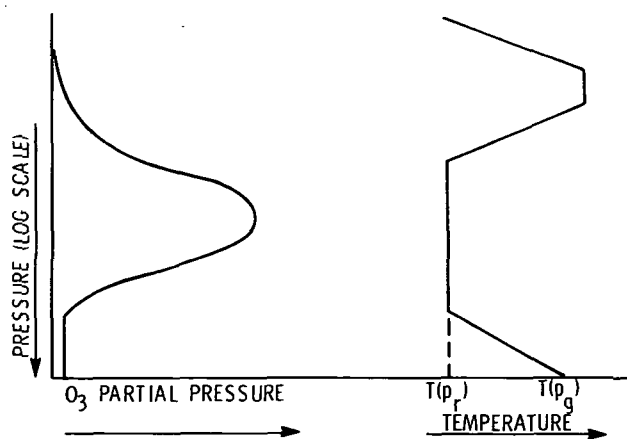


Figure 18.- Isothermal ozone layer with  $T(p_r) \neq T(p_g)$ .

APPENDIX B – Concluded

the same temperature as the ozone layer, that is, if  $T(p_g) = T(p_r)$ , then equation (B2) reduces to

$$\overline{L(\bar{\nu}_O, 0)} = B[\bar{\nu}_O, T(p_r)] \quad (B3)$$

which shows no structure. Such a spectrum contains no ozone information. Ways in which equation (B3) can occur are illustrated in figures 19 and 20. In figure 19 the underlying boundary is the earth's surface, and in figure 20 it is the top of a cloud layer for a completely overcast condition. If the troposphere is partly cloudy the effective lower boundary temperature, for a temperature profile like that of figure 20, will be at some intermediate value between the ground and tropopause temperatures. There would be structure in the ozone band for this partly cloudy condition, but the structure would not be as pronounced as for the clear-sky case. In fact, equation (B2) shows that as the value of  $T(p_g)$  approaches the value of  $T(p_r)$  the structure in the ozone band decreases and finally disappears when the two temperatures are equal.

A broad, nearly isothermal region in the middle and lower stratosphere is typical of the temperature profile in the high-latitude areas of the globe. Therefore, the entire range from full to no structure in the ozone band may be encountered at high latitudes depending upon the temperature profile and cloud conditions. Consequently, it sometimes may be difficult or impossible to determine ozone information from satellite measurements in the high-latitude regions.

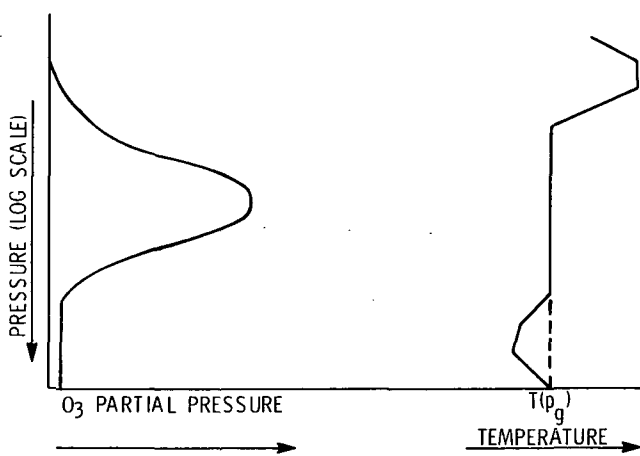


Figure 19.- Isothermal ozone layer with  $T(p_r) = T(p_g)$ .

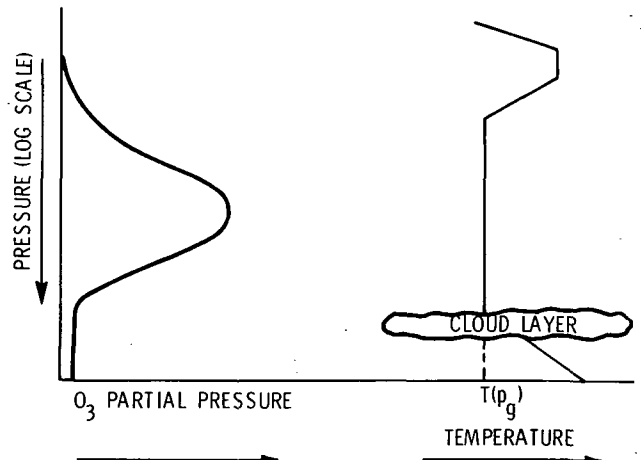


Figure 20.- Isothermal ozone layer with a total cloud cover in the troposphere.  $T(p_r) = T(p_g)$ .

## REFERENCES

1. Fabry, C.; and Buisson, M.: Absorption of Ultra-Violet Light by Ozone and Limit of Solar Spectrum. *J. Phys.*, vol. 3, ser. 5, Mar. 1913, pp. 196-206.
2. Chapman, S.: Theory of Upper Atmospheric Ozone. *Mem. Roy. Meteorol. Soc.*, vol. 3, June 1930, pp. 103-125.
3. Dobson, G. M. B.; Kimball, H. H.; and Kidson, E.: Amount of Ozone in the Earth's Atmosphere and Its Relation to Other Geophysical Conditions. IV. *Proc. Roy. Soc. (London)*, vol. A129, 1930, pp. 411-433.
4. Breiland, John G.: Vertical Distribution of Atmospheric Ozone and Its Relation to Synoptic Meteorological Conditions. *J. Geophys. Res.*, vol. 69, no. 18, Sept. 15, 1964, pp. 3801-3808.
5. Duardo, J. A.: Study To Develop a Technique for Measurement of High Altitude Ozone Parameters. Contract NAS 12-137, Electro-Optical Systems, Inc., May 15, 1967. (Available as NASA CR-80022.)
6. Paetzold, Hans-Karl: The Mean Vertical Ozone Distribution Resulting From the Photochemical Equilibrium, Turbulence and Currents of Air. *J. Atmos. & Terrest. Phys.*, vol. 3, no. 3, Apr. 1953, pp. 125-131.
7. Sticksel, Philip R.: The Vertical Distribution of Ozone Over Tallahassee, Florida. AFCRL-66-351, U.S. Air Force, June 15, 1964. (Available from DDC as AD 635 914.)
8. Godson, W. L.: Total Ozone and the Middle Stratosphere Over Arctic and Sub-Arctic Areas in Winter and Spring. *Quart. J. Roy. Meteorol. Soc.*, vol. 86, no. 369, July 1960, pp. 301-317.
9. Wulf, Oliver Reynolds: The Distribution of Atmospheric Ozone. *Proceedings of the Eighth Scientific Congress*, vol. 7, Amer. Meteorol. Soc., May 1940, pp. 439-446.
10. Normand, Charles: Some Recent Work on Ozone. *Quart. J. Roy. Meteorol. Soc.*, vol. 77, no. 333, July 1951, pp. 474-478.
11. Kellogg, William W.; and Schilling, Gerhard F.: A Proposed Model of the Circulation in the Upper Stratosphere. *J. Meteorol.*, vol. 8, no. 4, Aug. 1951, pp. 222-230.
12. Bekoryukov, V. I.: Computation of the Effect of Closed Air Circulation on the Equilibrium Distribution of Ozone in the Earth's Atmosphere. *Geomagnetism & Aeronomy*, vol. 5, no. 3, 1965, pp. 357-361.

13. Lindzen, Richard; and Goody, Richard: Radiative and Photochemical Processes in Mesospheric Dynamics: Pt. I, Models for Radiative and Photochemical Processes. *J. Atmos. Sci.*, vol. 22, no. 4, July 1965, pp. 341-348.
14. Anon.: Atmospheric Ozone Studies. Publ. 1348, Nat. Acad. Sci., 1966.
15. Singer, S. F.; and Wentworth, R. C.: A Method for the Determination of the Vertical Ozone Distribution From a Satellite. *J. Geophys. Res.*, vol. 62, no. 2, June 1957, pp. 299-308.
16. Sekera, Z.; and Dave, J. V.: Determination of the Vertical Distribution of Ozone From the Measurement of Diffusely Reflected Ultra-Violet Solar-Radiation. *Planetary & Space Sci.*, vol. 5, no. 2, June 1961, pp. 122-136.
17. Twomey, Sean: On the Deduction of the Vertical Distribution of Ozone by Ultraviolet Spectral Measurements From a Satellite. *J. Geophys. Res.*, vol. 66, no. 7, July 1961, pp. 2153-2162.
18. Dave, J. V.; and Mateer, Carlton L.: A Preliminary Study on the Possibility of Estimating Total Atmospheric Ozone From Satellite Measurements. *J. Atmos. Sci.*, vol. 24, no. 4, July 1967, pp. 414-427.
19. Herman, Benjamin M.; and Yarger, Douglas N.: Estimating the Vertical Atmospheric Ozone Distribution by Inverting the Radiative Transfer Equation for Pure Molecular Scattering. *J. Atmos. Sci.*, vol. 26, no. 1, Jan. 1969, pp. 153-162.
20. Anderson, Gail P.; Barth, Charles A.; Cayla, Francois; and London, Julius: Satellite Observations of the Vertical Ozone Distribution in the Upper Stratosphere. *Ann. Geophys.*, vol. 25, no. 1, 1969, pp. 341-345.
21. Frith, R.: Measuring the Ozone Above the Earth. *Discovery*, vol. 22, Sept. 1961, pp. 390-391.
22. Rawcliffe, R. D.; Meloy, G. E.; Friedman, R. M.; and Rogers, E. H.: Measurement of Vertical Distribution of Ozone From a Polar Orbiting Satellite. *J. Geophys. Res.*, vol. 68, no. 24, Dec. 15, 1963, pp. 6425-6429.
23. Miller, D. E.: The Measurement of Ozone From a Satellite. Paper presented at Brit. Interplanet. Soc., NATO Summer School (Cambridge), July 1969.
24. Hays, P. B.; and Roble, R. G.: Stellar Spectra and Atmospheric Composition. *J. Atmos. Sci.*, vol. 25, no. 6, Nov. 1968, pp. 1141-1153.
25. Conrath, Barney J.: Remote Sensing of Atmospheric Water Vapor and Ozone Using Interferometry. Specialist Conference on Molecular Radiation and Its Application to Diagnostic Techniques, NASA TM X-53711, Oct. 1967, pp. 277-296.

26. Sekihara, K.; and Walshaw, C. D.: The Possibility of Ozone Measurements From Satellites Using the 1043  $\text{cm}^{-1}$  Band. *Ann. Geophys.*, vol. 25, no. 1, 1969, pp. 233-241.
27. Prabhakara, C.: Feasibility of Determining Atmospheric Ozone From Outgoing Infrared Energy. *Mon. Weather Rev.*, vol. 97, no. 4, Apr. 1969, pp. 307-314.
28. Prabhakara, C.; Conrath, B. J.; Hanel, R. A.; and Williamson, E. J.: Remote Sensing of Atmospheric Ozone Using the 9.6  $\mu$  Band. *J. Atmos. Sci.*, vol. 27, no. 4, July 1970, pp. 689-697.
29. Chaney, L. W.; Loh, L. T.; and Surh, M. T.: A Fourier Transform Spectrometer for the Measurement of Atmospheric Thermal Radiation. Contract No. NASr-54(03), Coll. Eng., Univ. of Michigan, May 1967. (Available as NASA CR-85892.)
30. Chandrasekhar, S.: Radiative Transfer. Dover Pub., Inc., c.1960.
31. Kuhn, William R.; and London, Julius: Infrared Radiative Cooling in the Middle Atmosphere (30-110 km). *J. Atmos. Sci.*, vol. 26, no. 2, Mar. 1969, pp. 189-204.
32. Wark, D. Q.; and Fleming, H. E.: Indirect Measurements of Atmospheric Temperature Profiles From Satellites: I. Introduction. *Mon. Weather Rev.*, vol. 94, no. 6, June 1966, pp. 351-362.
33. Conrath, B. J.: Inverse Problems in Radiative Transfer: A Review. *Spacecraft Systems Education*, Vol. 2, Michal Lunc, P. Contensou, G. N. Duboshin, and W. F. Hilton, eds., Pergamon Press, Inc., 1968, pp. 339-360. (Also available as NASA TM X-55857, 1967.)
34. Gille, John C.: Inversion of Radiometric Measurements. *Bull. Amer. Meteorol. Soc.*, vol. 49, no. 9, Sept. 1968, pp. 903-912.
35. Clough, S. A.; and Kneizys, F. X.: Ozone Absorption in the 9.0 Micron Region. AFCRL-65-862, U.S. Air Force, Nov. 1965. (Available from DDC as AD 628 059.)
36. Drayson, S. Roland: Atmospheric Slant Path Transmission in the 15 $\mu$   $\text{CO}_2$  Band. NASA TN D-2744, 1965.
37. Drayson, S. Roland; and Young, Charles: Theoretical Investigations of Carbon Dioxide Radiative Transfer. 07349-1-F (Contract No. Cwb-11106), Coll. Eng., Univ. of Michigan, Aug. 1966.
38. Drayson, S. Roland: The Calculation of Long-Wave Radiative Transfer in Planetary Atmospheres. Nat. Sci. Found. Grant No. GP-4385, Coll. Eng., Univ. of Michigan, Nov. 1967. (Available as NASA CR-92998.)
39. Goody, R. M.: A Statistical Model for Water-Vapour Absorption. *Quart. J. Roy. Meteorol. Soc.*, vol. 78, no. 336, Apr. 1952, pp. 165-169.

40. Mayer, Harris: Methods of Opacity Calculations. LA-647 (Contract W-7405-ENG. 36), Los Alamos Sci. Lab., Univ. of California, Mar. 13, 1948.
41. Goldman, Aharon; and Kyle, Thomas G.: A Comparison Between Statistical Model and Line by Line Calculation With Application to the 9.6- $\mu$  Ozone and the 2.7- $\mu$  Water Vapor Bands. Appl. Opt., vol. 7, no. 6, June 1968, pp. 1167-1177.
42. Goody, R. M.: Atmospheric Radiation I. - Theoretical Basis. Clarendon Press (Oxford), 1964.
43. Armstrong, Baxter H.: Analysis of the Curtis-Godson Approximation and Radiation Transmission Through Inhomogeneous Atmospheres. J. Atmos. Sci., vol. 25, no. 2, Mar. 1968, pp. 312-322.
44. Walshaw, C. D.; and Rodgers, C. D.: The Effect of the Curtis-Godson Approximation on the Accuracy of Radiative Heating-Rate Calculations. Quant. J. Roy. Meteorol. Soc., vol. 89, no. 379, Jan. 1963, pp. 122-130.
45. Goody, Richard: The Transmission of Radiation Through an Inhomogeneous Atmosphere. J. Atmos. Sci., vol. 21, no. 6, Nov. 1964, pp. 575-581.
46. Gille, John C.; and Ellingson, Robert G.: Correction of Random Exponential Band Transmissions for Doppler Effects. Appl. Opt., vol. 7, no. 3, Mar. 1968, pp. 471-474.
47. Clough, Shepard A.; and Kneizys, Francis X.: Coriolis Interaction in the  $\nu_1$  and  $\nu_3$  Fundamentals of Ozone. J. Chem. Phys., vol. 44, no. 5, Mar. 1, 1966, pp. 1855-1861.
48. McCaa, David J.; and Shaw, John H.: The Infrared Absorption Bands of Ozone. AFCRL-67-0237, U.S. Air Force, Feb. 1967. (Available from DDC as AD 653 195.)
49. Benedict, William S.; and Calfee, Robert F.: Line Parameters for the 1.9 and 6.3 Micron Water Vapor Bands. ESSA Prof. Paper No. 2, U.S. Dep. Com., June 1967.
50. Alishouse, J. C.; Crone, L. J.; Fleming, H. E.; Van Cleef, F. L.; and Wark, D. Q.: A Discussion of Empirical Orthogonal Functions and Their Application to Vertical Temperature Profiles. Tellus, vol. 19, no. 3, 1967, pp. 477-482.
51. Craig, Richard A.: The Upper Atmosphere - Meteorology and Physics. Academic Press, Inc., c.1965.
52. Griggs, M.: Atmospheric Ozone. The Middle Ultraviolet: Its Science and Technology, A. E. S. Green, ed., John Wiley & Sons, Inc., c.1966, pp. 83-117.

53. Vassy, Arlette: Atmospheric Ozone. Advances in Geophysics, Vol. II, H. E. Landsberg and J. Van Mieghem, eds., Academic Press, Inc., 1965, pp. 115-173.
54. Hering, Wayne S., ed.: Ozonesonde Observations Over North America. Vol. I. AFCRL-64-30(1), U.S. Air Force, Jan. 1964. (Available from DDC as AD 435 873.)
55. Russell, James Madison, III: The Measurement of Atmospheric Ozone Using Satellite Infrared Observations in the 9.6 $\mu$ m Band. Contract No. NGR-23-005-376, Coll. Eng., Univ. of Michigan, July 1970. (Available as NASA CR-111566.)
56. Green, Alex E. S.: Attenuation by Ozone and the Earth's Albedo in the Middle Ultra-violet. Appl. Opt., vol. 3, no. 2, Feb. 1964, pp. 203-208.
57. Drayson, S. Roland: Errors in Atmospheric Temperature Structure Solutions From Remote Radiometric Measurements. Rep. No. 05863-4-T (Contract NASr-54(03)), High Altitude Eng. Lab., Univ. of Michigan, Dec. 1963. (Available as NASA CR-53120.)
58. Mateer, Carlton L.: A Study of the Information Content of Umkehr Observations. Tech. Rep. No. 2 (Nat. Sci. Found. Grant No. G-19131), Coll. Eng., Univ. of Michigan, Apr. 1964.
59. Hering, Wayne S.; and Borden, Thomas R., Jr., eds.: Ozonesonde Observations Over North America. Vol. 2. AFCRL-44-30(II), U.S. Air Force, July 1964. (Available from DDC as AD 604 880.)
60. Hering, Wayne S.; and Borden, Thomas R., Jr.: Ozonesonde Observations Over North America. Vol. 3. AFCRL-64-30(III), U.S. Air Force, Aug. 1965. (Available from DDC as AD 623 018.)
61. Hering, Wayne S.; and Borden, Thomas R., Jr.: Ozonesonde Observations Over North America. Vol. 4. AFCRL-64-30(IV), U.S. Air Force, Dec. 1967. (Available from DDC as AD 666 436.)
62. Regener, Victor H.: On a Sensitive Method for the Recording of Atmospheric Ozone. J. Geophys. Res., vol. 65, no. 12, Dec. 1960; pp. 3975-3977.
63. Regener, Victor H.: Measurement of Atmospheric Ozone With the Chemiluminescent Method. J. Geophys. Res., vol. 69, no. 18, Sept. 15, 1964, pp. 3795-3800.
64. London, Julius: A Study of the Atmospheric Heat Balance. AFCRC-TR-57-287, ASTIA No. 117227, Coll. Eng., New York Univ., July 1957.



POSTMASTER: If Undeliverable (Section 158  
Postal Manual) Do Not Return

*"The aeronautical and space activities of the United States shall be conducted so as to contribute . . . to the expansion of human knowledge of phenomena in the atmosphere and space. The Administration shall provide for the widest practicable and appropriate dissemination of information concerning its activities and the results thereof."*

—NATIONAL AERONAUTICS AND SPACE ACT OF 1958

## NASA SCIENTIFIC AND TECHNICAL PUBLICATIONS

**TECHNICAL REPORTS:** Scientific and technical information considered important, complete, and a lasting contribution to existing knowledge.

**TECHNICAL NOTES:** Information less broad in scope but nevertheless of importance as a contribution to existing knowledge.

**TECHNICAL MEMORANDUMS:** Information receiving limited distribution because of preliminary data, security classification, or other reasons. Also includes conference proceedings with either limited or unlimited distribution.

**CONTRACTOR REPORTS:** Scientific and technical information generated under a NASA contract or grant and considered an important contribution to existing knowledge.

**TECHNICAL TRANSLATIONS:** Information published in a foreign language considered to merit NASA distribution in English.

**SPECIAL PUBLICATIONS:** Information derived from or of value to NASA activities. Publications include final reports of major projects, monographs, data compilations, handbooks, sourcebooks, and special bibliographies.

**TECHNOLOGY UTILIZATION PUBLICATIONS:** Information on technology used by NASA that may be of particular interest in commercial and other non-aerospace applications. Publications include Tech Briefs, Technology Utilization Reports and Technology Surveys.

*Details on the availability of these publications may be obtained from:*

**SCIENTIFIC AND TECHNICAL INFORMATION OFFICE**

**NATIONAL AERONAUTICS AND SPACE ADMINISTRATION**  
Washington, D.C. 20546